AGU PUBLICATIONS

Journal of Advances in Modeling Earth Systems

RESEARCH ARTICLE
10.1002/2014MS000330

An updated treatment of soil texture and associated hydraulic properties in a global land modeling system

Gabriëlle J. M. De Lannoy[1,2], Randal D. Koster[1], Rolf H. Reichle[1], Sarith P. P. Mahanama[1,3], and Qing Liu[1,3]

[1]NASA Goddard Space Flight Center, Greenbelt, Maryland, USA, [2]Universities Space Research Association, Columbia, Maryland, USA, [3]Science Systems and Applications, Lanham, Maryland, USA

Key Points:
- Generated new global composite database of soil mineral and organic texture
- Derived soil hydraulic parameters for global land model simulations
- Reduced bias of simulated soil moisture versus in situ and satellite data

Correspondence to:
G. J. M. De Lannoy,
Gabrielle.DeLannoy@nasa.gov

Citation:
De Lannoy, G. J. M., R. D. Koster, R. H. Reichle, S. P. P. Mahanama, and Q. Liu (2014), An updated treatment of soil texture and associated hydraulic properties in a global land modeling system, *J. Adv. Model. Earth Syst.*, *06*, doi:10.1002/2014MS000330.

Received 2 APR 2014
Accepted 2 SEP 2014
Accepted article online 4 SEP 2014

Abstract The advent of new data sets describing soil texture and associated soil properties offers the promise of improved hydrological simulation. Here we describe the composition of a new soil texture data set and its implementation into a specific land surface modeling system, namely, the Catchment land surface model (LSM) of the NASA Goddard Earth Observing System version 5 (GEOS-5) modeling and assimilation framework. First, global soil texture composites are generated using data from the Harmonized World Soil Database version 1.21 (HWSD1.21) and the State Soil Geographic (STATSGO2) project, with explicit consideration of different levels of organic material. Then, the LSM's soil parameters are upgraded using the new texture data, with hydraulic parameters derived for the more extensive set of texture classes using pedotransfer functions. Other changes to the LSM parameters are included to further support simulations at increasingly fine resolutions. A suite of simulations with the original and new parameter versions shows modest yet significant improvements in the Catchment LSM's simulation of soil moisture and surface hydrological fluxes. The revised LSM parameters will be used for the forthcoming Soil Moisture Active Passive (SMAP) soil moisture assimilation product.

1. Introduction

In recent decades, improvements in the physical formulations and parameterizations of land surface models (LSMs) have led to improved global simulations of hydrological variables [*Balsamo et al*., 2009; *Reichle et al*., 2011; *Albergel et al*., 2012]. Such improvements are important for several reasons. LSMs, when used as part of an Earth modeling system, provide critical boundary conditions for weather and climate simulations [*Dirmeyer*, 2000; *Koster et al*., 2004]. LSMs also have many direct hydrological applications (e.g., streamflow prediction [*Wood and Lettenmaier*, 2006]), they provide the auxiliary information needed to produce satellite-based retrievals of geophysical quantities such as soil moisture [e.g., *Entekhabi et al*., 2010a; *Kerr et al*., 2012], and they serve as the modeling component for the land data assimilation systems that add value to either satellite-based retrievals or directly observed microwave signals [*Reichle et al*., 2014].

The climatology and temporal dynamics of simulated soil moisture are strongly affected by the soil parameters used in the simulation system [*Dharssi et al*., 2009; *Baroni et al*., 2010; *Comer and Best*, 2012], particularly the soil hydraulic parameters (SHPs). Models relying, for example, on the Richards' equation [*Richards*, 1931] to transport soil moisture between soil layers require information on, among other things, the hydraulic conductivity of the unsaturated soil and the functional relationship between degree of saturation and soil matric potential. These SHPs are strongly tied to soil texture. Sandy soils, for example, drain more easily than clay soils and have, for a given moisture content, a much higher hydraulic conductivity.

Historically, modeling groups have used spatial distributions of soil texture to infer the distributions of SHPs needed for their models. Under one common strategy, SHPs are extracted directly from lookup tables—a basic class of soil texture (e.g., sandy loam) for a land element is assumed based on field measurements, and the lookup table provides, for that class, the saturated hydraulic conductivity, the pore size distribution index, and all of the other SHPs needed for hydrological simulation (e.g., Global Soil Wetness Project, GSWP2 [*Dirmeyer and Oki*, 2002]). The lookup tables are generally built around a limited number of broad soil classes. The U.S. Department of Agriculture (USDA) "soil texture triangle" [*USDA Soil Survey Staff, Bureau of Plant Industry, Soils and Agricultural Engineering*, 1951], for example, maps the estimated percentages of

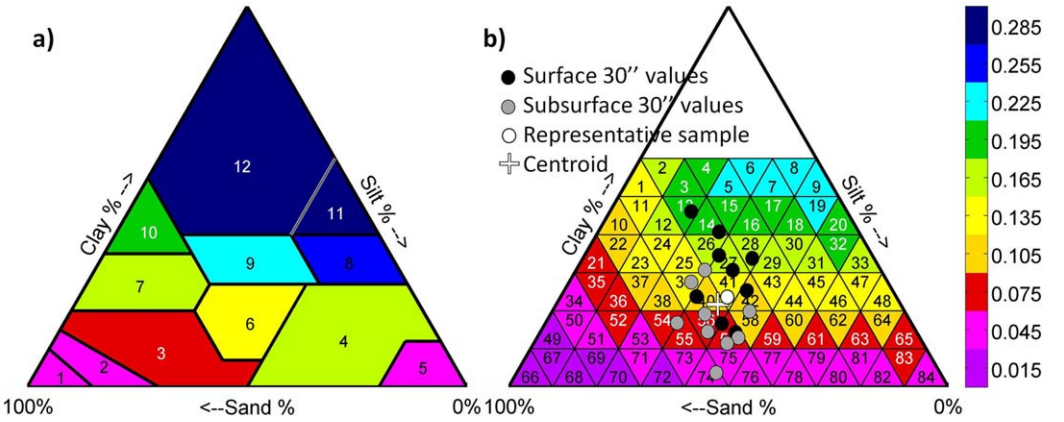

Figure 1. (a) Delineation of the 12 soil classes in the baseline version, based on the USDA soil classification. (b) Delineation of 84 mineral classes for one of three OC categories (category 1) in the revised version. The colors are keyed to the wilting point for each soil class. Figure 1b also illustrates the calculation of the representative mineral root zone (0-100 cm) class from the sand, silt, and clay percentages of the 30″ grid cells within one land model simulation element. In this context, the dots indicate the surface (0-30 cm) and subsurface (30-100 cm) percentages for individual 30″ grid cells, the white cross indicates their geometric centroid, and the white dot indicates the representative root zone soil sample that is closest to the geometric centroid of the (vertically) weighted dots. See text for details.

sand, silt, and clay at a given location into one of 12 defined soil classes (illustrated in Figure 1a), and lookup tables based on this or similar classifications are available in the literature [e.g., *Rawls et al*., 1982; *Cosby et al*., 1984].

While convenient, there is a fundamental problem with this strategy—within each broad soil class, the variability of SHPs can be very large and can even exceed the between-class variability [*McCuen et al*., 1981; *Loosvelt et al*., 2011]. Simply put, a soil classification scheme with a limited number of broad classes may be inadequate for defining the soil parameter variability that controls soil moisture behavior in nature. The problem is exacerbated if (as is common practice) modelers utilize tables that do not account for the presence of organic material in the soil. Organic material has a large impact on soil hydraulic and thermal parameters [*Rawls et al*., 2003]. Organic carbon (OC) affects the bulk density, hydraulic conductivity, and the range between wilting point and field capacity [*Kay et al*., 1997; *Rawls et al*., 2003; *Wesseling et al*., 2009]. *Rawls et al*. [2003] found a 25% increase in the accuracy of water retention estimates when OC is considered over that achieved using textural class information alone. OC also affects soil thermal properties: it has a low thermal conductivity and a high heat capacity [*Farouki*, 1981; *Letts et al*., 2000; *Lawrence and Slater*, 2000].

These limitations can be addressed through the use of pedotransfer functions (PTFs) [*Wösten et al*., 1999; *Wagner et al*., 2001; *Saxton and Rawls*, 2006; *Cronican and Gribb*, 2004]. The construction of these PTFs involves the analysis of soil hydrology data collected in the laboratory using multivariate regression or artificial neural networks; the equations that fall out of these analyses allow the direct conversion of sand, silt, clay, and organic matter percentages into the desired SHPs. Applying the PTFs to a more comprehensive catalog of soil textures (and organic content) leads to a more comprehensive lookup table for the SHPs and thus to a more complete representation of the variability of soil properties found in nature. Still, it is important to note that most PTFs are only valid within a specific range of texture and for limited organic matter contents. SHPs for highly organic soils are usually estimated separately [*Lawrence and Slater*, 2000; *Wösten et al*., 2001b].

The PTF approach is used in the present paper. It is important, however, to acknowledge the existence of other approaches to estimating SHPs, including those utilizing remotely sensed soil moisture retrievals [*Santanello et al*., 2007; *Pauwels et al*., 2009; *Salvucci and Entekhabi*, 2011; *Harrison et al*., 2012]. This type of approach (not discussed further here) comes with its own set of issues; the retrievals, for example, inherently include some assumption about soil texture, which may be inconsistent with the texture assumed in the land surface model, and the optimized SHP values and the feasibility of a global calibration effort will depend on the choice of the calibration algorithm and on the coverage and quality of the remote sensing data.

While the main focus of this paper is on improving the SHPs for hydrological simulations, the update in soil texture is also beneficial as input to diagnostic simulations of, for example, brightness temperature [*De*

Lannoy et al., 2013] or to retrieve soil moisture from satellite-based observations of microwave radiation [*Entekhabi et al*., 2010a; *Kerr et al*., 2012]. The composite new soil texture information presented herein will provide key background information for the creation of soil moisture products that will be delivered with the upcoming Soil Moisture Active Passive (SMAP) mission.

Section 2 describes how we put together a global soil texture data set by merging, in a sensible way, existing data sets from multiple sources. Our construction of a more comprehensive lookup table for SHPs is also described in section 2. The application of the PTFs to the merged global soil texture data results in global distributions of SHPs, and the impacts of these new parameter values, along with some additional changes, on simulated hydrological variables are evaluated in section 3. The land model utilized in the evaluations is the Catchment land surface model (Catchment LSM [*Koster et al*., 2000]), a part of the Goddard Earth Observing System Model version 5 (GEOS-5) framework developed by the Global Modeling and Assimilation Office at the NASA Goddard Space Flight Center. GEOS-5 is used to generate widely used reanalysis data products, including the Modern-Era Retrospective analysis for Research and Applications (MERRA) [*Rienecker et al*., 2011], its supplemental land surface reanalysis (MERRA-Land) [*Reichle et al*., 2011], and the forthcoming MERRA version 2 reanalysis (MERRA2). GEOS-5 is further used to generate near-real time atmospheric data assimilation and forecast products (https://gmao.gsfc.nasa.gov/products). The "baseline" simulations in this paper use settings similar to those used in MERRA-Land and MERRA2. The land surface system in MERRA-Land includes some upgrades compared to MERRA and is similar to the land surface component of MERRA2 (with small differences discussed below), but none of these systems yet include the update in soil texture and SHPs that will be detailed in this paper. The Catchment LSM will also be used to generate the SMAP Level 4 Surface and Root Zone Soil Moisture data product (L4_SM [*Reichle et al*., 2012]). Simulations with the "revised" GEOS-5 texture and SHP information presented here closely mimic the settings that are expected for the initial version of the SMAP L4_SM product.

We emphasize that the choices made in the composition of the new soil texture database and the derivation of the new SHPs are largely driven by the particular needs of our global land surface modeling system. Given the current state of modeling, we leave for future consideration a number of other potentially important aspects of the problem, including soil chemical composition [*Shangguan et al*., 2014], high vertical resolution soil texture profiles [*Dai et al*., 2013], the presence of rocks [*Cosh et al*., 2008] and other impurities, tropical soils [*Minasny and Hartemink*, 2011], soil heat dynamics [*Lawrence and Slater*, 2000], and soil management. These issues will undoubtedly require more attention in soil data sets as global land models evolve, and they are indeed starting to garner attention, as indicated by the noted studies. For our purposes, the more limited reconfiguration of our representation of soils, as described herein, is nevertheless still substantial, and the impacts found here should have relevance beyond GEOS-5. That is, given the current state of the art in global land surface modeling, our findings should have relevance to global modeling efforts in general.

2. Updated Classification of Soils and Their Associated Hydraulic Properties

2.1. Updated Soil Texture and Organic Carbon Maps

The soil texture map used to derive SHPs in the original, "baseline" versions of the GEOS-5 Catchment LSM is based on the National Oceanic and Atmospheric Administration National Geophysical Data Center (NGDC [*Reynolds et al*., 2000]) texture data, which is essentially an interpretation of the Food and Agriculture Organization (FAO)—United Nations Educational, Scientific and Cultural Organization (UNESCO) Soil Map of the World [*FAO/UNESCO*, 1971–1981]. For our new soil classification, we upgrade the texture information with more recent or more accurate (e.g., more highly resolved) information, effectively merging two sources of mineral and organic texture data into a single global surface and root zone texture map. Recently, *Shangguan et al*. [2014] generated a composited global soil database with mineral texture and chemical properties at eight soil layers to a depth of 2.3 m. Our focus here is somewhat different, for we aim to produce a composited texture data set that is especially amenable to the robust production of SHPs for a typical global land surface modeling system. Given the uncertainty associated with spatially extrapolating local soil profile information and the associated SHPs, we limit the information to surface and root zone characteristics only. Furthermore, we added improved soil texture information over the U.S., which helps remote sensing (e.g., SMAP) and modeling evaluation efforts over this domain.

Our first data source is the high-resolution State Soil Geographic (STATSGO2) [*NRCS Soil Survey Staff, USDA*, 2012] texture data set, which contains information for the U.S. (including Alaska, Hawaii, and Puerto Rico).

STATSGO2 soil survey areas are mapped at a scale of 1:250,000 across the conterminous U.S. and 1:1,000,000 in Alaska, with a minimal map unit size delineation of 2500 acres.

The second contributing data set is the Harmonized World Soil Databank version 1.21 (HWSD1.21) [*FAO/IIASA/ISRIC/ISSCAS/JRC*, 2012]. The HWSD1.21 combines the European soil database, the soil map of China, and numerous regional databases with the information contained in the FAO-UNESCO Soil Map of the World [*FAO/UNESCO*, 1971–1981]. This data set covers most of the globe with a nominal resolution of 30″ (~1 km). The HWSD1.21 does not yet include the STATSGO2 database for the U.S. and similar national databases for Canada and Australia, but the inclusion of these databases is foreseen in future HWSD updates. To satisfy our immediate need for an updated soil data set for the SMAP mission, we implemented the merger of HWSD1.21 and STATSGO2 ourselves.

Both contributing data sets provide information on the sand, silt, and clay fractions of the soil, as well as on the organic carbon (OC) or organic matter (OM) content in a surface layer (0–30 cm) and a subsurface layer (30–100 cm). Where needed, OM (weight % of organic molecules in the bulk soil) is converted to OC (weight % of carbon itself) using the conversion OM = 1.72 OC, based on the fact that soil organic matter contains approximately 58% carbon. We only extract sand and clay from the STATSGO2 soil databank. Silt percentage was computed as the residual to ensure that the sum of mineral components adds up to 100%. (Note that in the original data set, the sum of the sand, silt, and clay percentages occasionally and erroneously differs from 100%.)

We construct the merged data set on a global 30″ grid, which matches that of the HWSD1.21 database. Prior to merging the HWSD1.12 and STATSGO2 texture data, the vector (shape) information in the STATSGO2 data set is mapped to the 30″ resolution by selecting the dominant mineral soil texture (based on areal coverage) and by averaging the organic material across the shapes that fall within each 30″ grid cell. The dominant mineral soil texture is selected in order to ensure that we use soil properties corresponding to those of a soil that actually exists within the grid cell.

The merged product is constructed by using STATSGO2 data where available. Outside of the STATSGO2 area, HWSD1.21 information is used. This approach is taken for mineral texture and OC separately; if, for example, STATSGO2 does provide information on OC, but does not provide complete information on sand and clay, we use OC from STATSGO2 and mineral texture from HWSD1.21. However, at each location, we require that the surface and subsurface soil information are taken from the same data source.

When information for either the surface or the subsurface layer is missing, the information is inferred from that of the available layer. For mineral texture, the available layer's information is applied directly to the missing layer, while for OC, we assume a subsurface-to-surface ratio of 0.3, based on a global calculation of this ratio at locations with complete OC profile information. At 30″ grid cells where both the surface and subsurface information is missing for the mineral texture, the data are filled by assigning the texture of the 30″ grid cell that has the median sand of all the available textures in the vicinity. Similarly, the 30″ grid cells with missing OC values are filled using the median OC value of the available OC in the vicinity. Alternatively, some areas with missing data could perhaps be assigned the soil properties of dune sand or salt flats as in *Batjes* [2012]. But note that this approach is problematic in the subsurface layer where data are often missing in mountainous areas where soil may not exist because of solid rock formations. We fill the missing value anyway because the global land surface model requires spatially complete fields of soil texture. The depth to bedrock parameter will, in any case, limit the soil thickness in rocky areas. In the future, if the assignment of "rock" or other nonsoil surface types is desired in certain locations, the filled-in soil parameters at those locations can be easily overwritten.

The areal contribution of each data source to the final merged mineral texture field is illustrated in Figure 2. Similar areal contributions are found for OC (not shown).

2.2. Assignment of Dominant Texture to Land Surface Model Elements

The simulation elements utilized by a global LSM are generally much larger than the 30″ resolution of the soil texture data set. For example, the simulations in this study will be performed at either 36 or 9 km resolution. Thus, prior to determining SHPs for a given element, the "representative" soil class for the element must be established. In fact, two soil classes are established for each simulation element, one for the 0–30 cm surface zone and another for the combined 0–100 cm layer, which includes both the surface and the subsurface layer. In keeping with the Catchment model terminology, we also refer to this combined layer as

the "root zone" layer. The surface texture is used only to parameterize surface layer moisture transport time scales, whereas the root zone class determines all other soil parameters. The selection of an element's soil class for either vertical zone is accomplished in two steps.

The first step involves identifying the dominant organic carbon category (OC category) for the land simulation element. We define a total of four OC categories. Three of these categories contain low to moderate levels of OC, which can be used directly in PTFs:

1. $0\% \leq \mathrm{OC} < 0.40\%$ (nominal value $= 0.26\%$),

2. $0.40\% \leq \mathrm{OC} < 0.64\%$ (nominal value $= 0.46\%$), and

3. $0.64\% \leq \mathrm{OC} < 8.72\%$ (nominal value $= 1.12\%$),

where the percentage units are in terms of weight. The fourth OC category, "peat," encompasses all soils with OC levels $\geq 8.72\%$ (or, equivalently, $\mathrm{OM} \geq 15\% = 8.72\% \times 1.72$). Soils in this "peat" category are assigned a distinct set of SHPs (see below). The OC boundaries indicated for the first three categories are the tercile boundaries for all OC content values below a maximum threshold of 8.72% by weight, derived from a weighted global distribution in the surface and subsurface soil at 30″ resolution and prior to any spatial gap filling. The nominal value corresponds to the median OC value for each category. We have verified (not shown) that three OC categories are indeed sufficient to capture important sensitivities of SHPs to OC content in the low to moderate range.

With these categories defined for each 30″ grid cell in the data set, the number of grid cells of each OC category lying within the LSM simulation element is determined. The OC category with the greatest number of grid cells in the simulation element is deemed the OC category for the element as a whole and only those grid cells with OC values in the dominant OC category are retained in the next step.

The second step in determining the LSM simulation element's representative soil class involves establishing a representative "mineral class" for the element. The approach used here is built on the soil texture triangle, which we now partition into small triangles representing refined soil classes with increments of 10% in the sand, silt, and clay percentages, as illustrated in Figure 1b. This results in 84 small triangles with up to 60% of clay content. (For higher clay contents, many of the PTFs described below are invalid.) Each 30″ grid cell lying within the dominant OC category of a land simulation element is associated with a particular percentage of sand, silt, and clay and can be represented by a unique dot in the triangle, as illustrated in Figure 1b. The figure shows how a root zone (0–100 cm) soil class is determined based on a weighted combination of surface (0–30 cm) and subsurface (30–100 cm) 30″ samples. We determine the single "representative" sample closest to the geometric centroid (illustrated by a cross) of all individual 30″ grid cell samples. If that representative sample (identified by the white dot) lies inside one of the 84 small triangles in Figure 1b, then that triangle is taken to be the mineral class for the land simulation element. (Note that the triangle associated with the representative sample might differ from the triangle that is associated with the centroid, and this is acceptable; we want to ensure, as much as possible, that we choose a soil texture known to exist somewhere

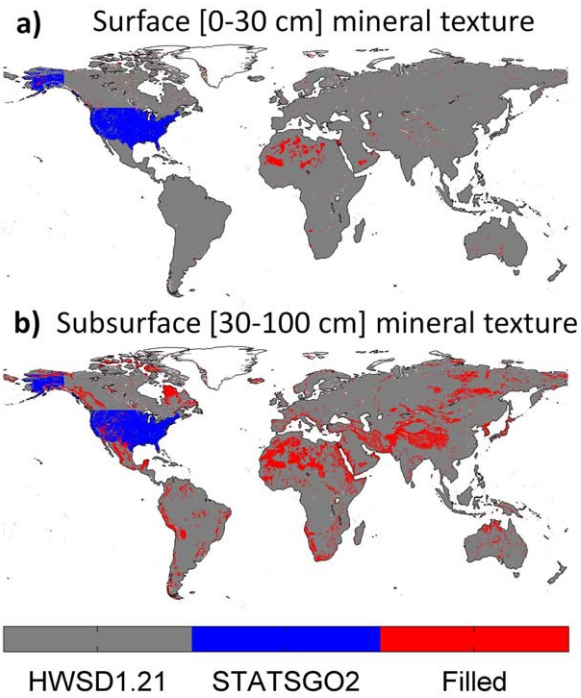

Figure 2. Contribution of individual soil data sources to the revised global composite soil texture map (30″) for the (a) surface and (b) subsurface layer.

within the element.) If the representative sample lies above the small triangles (amounting to less than 1% of the total land area), the nearest small triangle is chosen as the mineral class. The same procedure is followed to determine the surface mineral class, but using surface information only (i.e., without any weighting of surface and subsurface information).

The representative OC category and mineral class for an element together categorize the element as being in one of 253 possible soil classes: 84 mineral classes are defined for each of the first three OC categories, with an additional 253rd class representing "peat." Combined with the PTFs described below, this allows 253 distinct representations of soil hydraulic behavior in the model. The original GEOS-5 soil characterization, in contrast, defined only 12 distinct soil classes, as indicated in Figure 1a, and thus only 12 representations of hydraulic behavior. Also, in the original classification, distinct OC categories were not considered.

The above classification of soil classes is based purely on the mineral and organic composition of the soil. Alternative classification strategies exist; the soils could be stratified, for example, based on effective hydraulic properties [*Bormann*, 2010]. Such alternative approaches, however, might preclude other applications of the data set, such as its use in associated radiative transfer modeling efforts, for which explicit soil textures are required. For consistency with such other efforts, the texture-based classification described above has a distinct advantage.

2.3. Utilization of Pedotransfer Functions (PTFs)

2.3.1. Parameters to Estimate

In this paper, we focus on the determination of parameters that relate soil moisture content (θ) to matric potential (ψ) and hydraulic conductivity (K) within each land simulation element. The Catchment LSM utilizes the following relationships [*Campbell*, 1974]:

$$\psi/\psi_s = (\theta/\theta_s)^{-b} \text{ and} \tag{1}$$

$$K = K_s(\theta/\theta_s)^{2b+3} \tag{2}$$

where θ_s (m^3/m^3) is the soil moisture content at saturation, ψ_s (m H_2O) is the air entry pressure, b is an empirical parameter that describes the shape of the water retention curve, and K_s (mm/s) is the saturated hydraulic conductivity. Given this design, we focus here on the estimation of the parameters b, θ_s, ψ_s, and K_s, as well as on the wilting point wp (m^3/m^3), a parameter that affects evaporation and, indeed, the minimum attainable soil moisture in the model.

2.3.2. PTF Source

In the original ("baseline") treatment of soils in the Catchment LSM, the soil in a simulation element was categorized as one of 12 classes, and a lookup table (GSWP2 [*Dirmeyer and Oki*, 2002], adapted from *Cosby et al*. [1984]) was used to translate the soil class into values of b, θ_s, ψ_s, K_s, and wp. Here we apply PTFs to the 252 soil classes with moderate OC contents, functions that relate these parameters to soil texture and OC content. For the 253rd "peat"-class, separate lookup values are used. We obtain, as a result, a substantially expanded lookup table based on 253 soil classes.

Numerous examples of PTFs are available in the literature. *Cosby et al*. [1984], *Rawls and Brakensiek* [1989], and *Saxton and Rawls* [2006], for example, provide PTFs built from a collection of North-American soil samples, and *Wösten et al*. [1999, 2001a] provide PTFs based on European soil samples. These PTFs differ mainly in their required input parameters and in the underlying functional forms assumed for $\psi(\theta)$ and $K(\theta)$.

For our purposes, we require PTFs that account for the presence of organic matter, which suggests that the PTFs of *Saxton and Rawls* [2006] and *Wösten et al*. [2001a] may be suitable. We choose the PTFs of *Wösten et al*. [2001a], because those of *Saxton and Rawls* [2006] are built on the assumption of a three-piece $\theta(\psi)$ relationship, whereas those of *Wösten et al*. [2001a] assume a *van Genuchten* [1980] relationship, which has parameters that can more easily be interpreted in terms of those in equations (1) and (2).

2.3.3. Soil Bulk Density Calculation

The sand, silt, and clay percentages and OC content for a given vertical zone of a land simulation element are defined by the soil class chosen in Figure 1b. The soil bulk density (ρ_b) is another critical input into the *Wösten et al*. [2001a] PTF calculations and is calculated here as follows.

We first obtain an initial estimate of soil moisture content at saturation (θ_s^*) using the PTF of *Saxton and Rawls* [2006], which does not require information on bulk density and calculates θ_s^* while accounting for OC

Table 1. Derivation of the Soil Bulk Density ρ_b[a]

SHP	Units	PTF
θ_{33t}	m^3/m^3	$= -0.251 \times sand\_f + 0.195 \times clay\_f + 0.011 \times OM + 0.006 \times sand\_f \times OM - 0.027 \times clay\_f \times OM + 0.452 \times sand\_f \times clay\_f + 0.299$
θ_{33}	m^3/m^3	$= \theta_{33t} + (1.283 \times \theta_{33t}^2 - 0.374 \times \theta_{33t} - 0.015)$
$\theta_{(s\text{-}33)t}$	m^3/m^3	$= 0.278 \times sand\_f + 0.034 \times clay\_f + 0.022 \times OM - 0.018 \times sand\_f \times OM - 0.027 \times clay\_f \times OM - 0.584 \times sand\_f \times clay\_f + 0.078$
$\theta_{(s\text{-}33)}$	m^3/m^3	$= \theta_{(s\text{-}33)t} + (0.6360 \times \theta_{(s\text{-}33)t} - 0.107)$
θ_s^*	m^3/m^3	$= \theta_{33} + \theta_{(s\text{-}33)} - 0.097 \times sand\_f + 0.043$
$\boldsymbol{\rho_b}$	g/cm^3	$= (1 - \theta_s^*/0.93)\ \rho_{min}/[1 + (OM/100)\ (\rho_{min}/\rho_{OM} - 1)]$ (equation (5))

[a]The bold symbols in the left column indicate the final variables, whereas all other variables are auxiliary. The initial estimate of the soil moisture at saturation (θ_s^*) uses *Saxton and Rawls* [2006] PTFs, with sand_f, silt_f, clay_f in weight fractions and OM in weight%. This auxiliary variable θ_s^* is used to estimate ρ_b. The auxiliary variable θ_{33} is the solution for moisture at a tension of −33 kPa (θ_{33t} is a temporary first solution), $\theta_{(s\text{-}33)}$ is the solution for moisture at a tension between saturation and −33 kPa ($\theta_{(s\text{-}33)t}$ is a temporary first solution).

(Table 1). If the soil consisted only of mineral components, then an estimate of the bulk density would be $\rho_b = (1 - \theta_s^*).\rho_{min}$, where ρ_{min} is the actual density of mineral particles. (Note that this approach is taken in the ρ_b calculation in the HWSD.) Instead, we estimate the porosity as $\varphi = \theta_s/0.93$ [*McKenzie et al*., 2002], and account for the presence of organic material in the bulk density. If f_{OM} represents the volumetric fraction of organic material, and if ρ_{min} and ρ_{OM} represent the average densities of mineral particles and organic matter, respectively, then we have:

$$\rho_b = (1 - f_{OM} - \varphi)\ \rho_{min} + f_{OM}\ \rho_{OM} \tag{3}$$

The volumetric fraction f_{OM} is related in a straightforward way to the mass fraction of organic matter, OM/100 (which itself is directly related to a nominal OC-value for the considered soil class), according to

$$\begin{aligned} f_{OM} &= \text{volume of organic material}/\text{volume of soil} \\ &= [\text{grams organic material}/\rho_{OM}]/[\text{grams soil}/\rho_b] = OM/100(\rho_b/\rho_{OM}) \end{aligned} \tag{4}$$

Combining (3) with (4) produces an equation that allows the calculation of bulk density accounting for the organic mass fraction:

$$\rho_b = (1 - \varphi)\rho_{min}/[1 + (OM/100)\ (\rho_{min}/\rho_{OM} - 1)] \tag{5}$$

In our calculations, we take $\rho_{min} = 2.65\ g/cm^3$ (a reasonable value for soils that are predominantly quartz, feldspars, micas and colloidal silicates) and $\rho_{OM} = 1.3\ g/cm^3$ (from a range of approximately $0.9 - 1.4\ g/cm^3$) as practical values used in literature [*McKenzie et al*., 2002]. This approach results in slightly lower bulk densities than what is obtained when using $\rho_b = (1 - \theta_s^*).\rho_{min}$ (as provided in the HWSD). The effect of our adjusted ρ_b calculation on the SHPs is small and only noticeable for soil classes with higher organic contents (OC 3).

2.3.4. PTF-Derived and Lookup Parameters

Table 2 provides the *Wösten et al*. [2001a] PTFs, which are used here and which require silt and clay percentages, OC content, and soil bulk density as inputs. These PTFs facilitate the calculation of SHPs for the topsoil layer by using "topsoil=1." Similarly, SHPs for the subsoil layer are obtained by using "topsoil=0." Since our definition of the root zone layer includes the surface soil layer, we choose to apply the PTFs with "topsoil=1," for both the surface layer and the root zone layer. Since the original *Wösten et al*. [2001a] PTFs generate parameters for the *van Genuchten* [1980] water retention curve but the Catchment model uses the *Campbell* [1974] curve, the bottom half of Table 2 includes both numerical transformations that are part of the *Wösten et al*. [2001a] PTFs to obtain the *van Genuchten* [1980] parameters (θ_s, α, n, K_s) and transformations to obtain the *Campbell* [1974] parameters (θ_s, ψ_s, b, K_s). The latter are described in, for example, *Wagner et al*. [2001]. For example, the pore size distribution measure n is part of the *van Genuchten* [1980] equation and is directly related to the b parameter in the *Campbell* [1974] equation. As illustrated in Figure 3, the two curves are very similar. The key differences are: (i) the *Campbell* [1974] curve does not require an estimate of the residual soil moisture, and (ii) unlike the smooth *van Genuchten* [1980] curve, the *Campbell* [1974] curve has a sharp discontinuity in suction, or tension, near saturation.

As noted above, the 253rd soil class, peat, represents all elements for which the soil organic matter exceeds 15% of the bulk soil mass. The soil parameters for this 253rd class are not derived with PTFs but are instead

Table 2. Derivation of SHP Using *Wösten et al.* [1999, 2001a] PTFs With sand, silt, clay, and OM in weight% and ρ_b in g/cm^3[a]

SHP	Units	PTF
θ_s	m^3/m^3	$= 0.7919 + 0.001691 \times clay - 0.29619 \times \rho_b - 0.000001491 \times silt^2 + 0.0000821 \times OM^2 + 0.02427 \times clay^{-1} + 0.01113 \times silt^{-1} + 0.01472 \times \ln(silt) - 0.0000733 \times OM \times clay - 0.000619 \times \rho_b \times clay - 0.001183 \times \rho_b \times OM - 0.0001664 \times topsoil \times silt$
α*		$= -14.96 + 0.03135 \times clay + 0.0351 \times silt + 0.646 \times OM + 15.29 \times \rho_b - 0.192 \times topsoil - 4.671 \times \rho_b^2 - 0.000781 \times clay^2 - 0.00687 \times OM^2 + 0.0449 \times OM^{-1} + 0.0663 \times \ln(silt) + 0.1482 \times \ln(OM) - 0.04546 \times \rho_b \times silt - 0.4852 \times \rho_b \times OM + 0.00673 \times topsoil \times clay$
n*		$= -25.23 - 0.02195 \times clay + 0.0074 \times silt - 0.1940 \times OM + 45.5 \times \rho_b - 7.24 \times \rho_b^2 + 0.0003658 \times clay^2 + 0.002885 \times OM^2 - 12.81 \times \rho_b^{-1} - 0.1524 \times silt^{-1} - 0.01958 \times OM^{-1} - 0.2876 \times \ln(silt) - 0.0709 \times \ln(OM) - 44.6 \times \ln(\rho_b) - 0.02264 \times \rho_b \times clay + 0.0896 \times \rho_b \times OM + 0.00718 \times topsoil \times clay$
K_s*		$= 7.755 + 0.0352 \times silt + 0.93 \times topsoil - 0.967 \times \rho_b^2 - 0.000484 \times clay^2 - 0.000322 \times silt^2 + 0.001 \times silt^{-1} - 0.0748 \times OM^{-1} - 0.643 \times \ln(silt) - 0.01398 \times \rho_b \times clay - 0.1673 \times \rho_b \times OM + 0.02986 \times topsoil \times clay - 0.03305 \times topsoil \times silt$
α	1/m	$= \exp(\alpha^*)$
n		$= \exp(n^*) + 1$
K_s	m/s	$= 0.01 \exp(K_s^*)/(3600 \times 24)$
b		$= 1/(n - 1)$
ψ_s	m H_2O	$= -0.01/\alpha$

[a]Use topsoil=1 to obtain SHPs for the (0–30 cm) surface layer and topsoil=0 to obtain SHPs for the (30–100 cm) subsurface layer. The bold symbols in the left column indicate final *Campbell* [1974] SHP values, whereas all other variables are temporary in the calculation of the SHP. The *van Genuchten* [1980] parameters are θ_s, α, n, and K_s; the *Campbell* [1974] parameters are θ_s, ψ_s, b, and K_s.

based on parameters reported in the Staring series [*Wösten et al.*, 2001b]. The values for θ_s, ψ_s, b, and K_s are taken from the classes "peat_B16" and "peat_O17" in that reference for the surface soil and subsurface soil, respectively. These values are within the range of parameter values reported for different organic classes by *Letts et al.* [2000], *Wösten et al.* [2001a], and *Balsamo et al.* [2009].

The appendix (Table A1) lists the SHPs for all soil classes, using the *Wösten et al.* [2001a] PFTs for the first 252 classes and lookup values for the peat class (class 253). The soil class numbers for OC category 1 (1–84) are shown in Figure 1b; the numbers for OC category 2 (85–168) and category 3 (169–252) follow the same ordering in the soil triangle. Table A1 also includes the wilting point (wp) and field capacity (fc), obtained by inverting the *Campbell* [1974] formulation at −1500 and −33 kPa underpressure (equivalent to pF = 4.3 and 2.5), respectively, as illustrated in Figure 3 for a particular class. Finally, the colors in Figure 1 illustrate the wilting point associated with the original soil classes and the revised soil classes belonging to OC category 1.

2.4. Additional Modifications Related to Soil Hydraulic Parameters

Once the SHP values are determined for each element as described above, they are processed into additional Catchment model-specific parameters—parameters that describe, for example, the subgrid distribution of soil moisture as a function of total water storage and topography. We do not discuss this processing further here (see *Ducharne et al.* [2000] for more details) except to indicate three additional changes made relative to the original method of processing the parameters. The changes are summarized in Table 3, and simulations designed to quantify the impacts of the changes will be discussed in section 3.

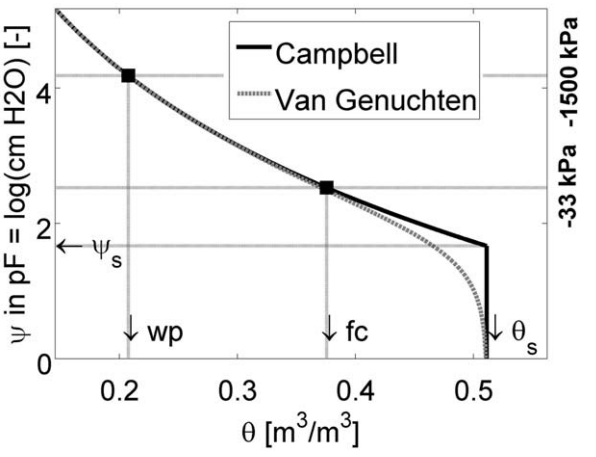

Figure 3. Campbell and Van Genuchten retention curves for soil class 17 (46.7% clay, 17% sand, 0.26% OC), with an indication of relevant parameter values ($\psi_s = -0.46$ m (pF = 1.7), $\theta_s = 0.51$ m^3/m^3). The curvature of the Campbell retention curve for $\theta < \theta_s$ is determined by the parameter b = 6.43. The retention curve relates soil moisture content (θ) to matric potential (ψ), with the latter here expressed in pF. The wilting point (wp) and field capacity (fc) are inverted from the Campbell retention curve at −1500 kPa (pF = 4.3) and −33 kPa (pF = 2.5), respectively.

The first change involves the assumed depth-to-bedrock. In the new version, bedrock depths at high resolution are spatially interpolated from the 1° × 1° resolution data set used in GSWP2 [*Dirmeyer and Oki*, 2002], and the minimum depth-to-bedrock that can be assigned is increased to 1.334 m, which allows a globally uniform root zone depth of 1 m. This change leads to an increase in water

Table 3. Overview of the Baseline (BL, BLM2) and Revised (REV) Versions of the Catchment Model Parameters

Parameter Version	BL	BLM2	REV
GEOS-5 systems	MERRA, MERRA-Land	MERRA2	SMAP L4_SM
Mineral texture	NGDC	NGDC	STATSGO2 + HWSD1.21
Organic carbon	No	No	Yes
SHP, PTFs	Adapted from *Cosby et al.* [1984]	Adapted from *Cosby et al.* [1984]	*Wösten et al.* [2001a]
Minimum soil depth (mm)	1000	1334	1334
Depth-to-bedrock interpolation	No	Yes	Yes
ν (vertical decay factor) (1/m)	2.17	1.0	1.0
Minor change to soil moisture transport calculation	No	Yes	Yes

holding capacity in many parts of the world. The spatial interpolation prevents adverse spatial discontinuities in higher-resolution land model simulations.

The second change involves the Catchment LSM's treatment of hydraulic conductivity for the base flow calculation. For the calculation of the time scales of moisture transport between soil reservoirs, the Catchment LSM utilizes a vertically uniform hydraulic conductivity in the root zone, with K_s (for the new version) set to the root zone value found as described above. However, the LSM's calculation of the water table distribution and the associated base flow production requires an assumption, derived from the TOPMODEL framework [*Sivapalan et al.*, 1987], that K_s varies with depth according to:

$$K_s(z) = K_s(0)\ \exp(-\nu z) \tag{6}$$

where z (m) is the depth into the soil and ν (1/m) is a tunable decay factor. For these calculations only, we assume that the root zone value of K_s applies at a 2 m depth and compute a corresponding value of $K_s(0)$. At this time, based on tuning and other considerations, the new version uses a universal value of 1.0 (1/m) for ν, in contrast to the value of 2.17 (1/m) used in the original version.

The third change pertains to a minor modification imposed in the soil moisture transport calculation. It is mentioned here for completeness; tests show that the change, which was imposed to prevent instabilities stemming from the relatively fast drainage associated with a handful of our new soil textures, does not have an important impact on our simulated fields.

2.5. Overview of Changes in Soil Texture, Organic Carbon, and Hydraulic Properties

Global maps for the surface and root zone soil classes derived for the revised parameter version at 36 km resolution are shown in Figure 4. The distinct colors highlight the different organic classes, whereas darker shadings per color indicate higher clay contents. The peat class is mainly found in the northern latitudes and Indonesia. Most of the globe has a surface soil class within organic class III, i.e., with more than 0.64% OC, except in very dry areas with little or no vegetation. In contrast, the root zone soil classes cover all three moderate organic classes, with large areas containing less than 0.40% OC. The area covered by STATSGO2 shows higher surface OC in Alaska than any of the other data sources (not shown); the STATSGO 2 values are found to be in line with independent measurements [*Liu et al.*, 2013].

The characterization of soil in the revised version differs significantly from that in the baseline version. The plots for 36 km resolution root zone mineral texture in Figures 5a–5d show that the global distribution of the texture is changed regionally. Globally averaged, the revised version has slightly more sand (Figure 5b) and slightly less clay (Figure 5d) than the baseline version.

This change, along with aforementioned changes in the approaches used to translate textures into soil parameters, has a clear impact on b, θ_s, ψ_s, K_s, and wp, with the distributions for θ_s and wp illustrated in Figures 5e–5h, again at 36 km resolution. The revised θ_s is locally increased in areas with high OC contents (Figures 5e and 5f). The global average of the wilting point wp decreased from 0.17 m^3/m^3 in the baseline to 0.11 m^3/m^3 in the revised parameter set (Figures 5g and 5h). This decrease in wp is explained both by a slight increase in sand and by the *Wösten et al.* [2001a] PTFs for "topsoil = 1," which yield retention curves with lower values for wp than the GSWP2 lookup table [*Dirmeyer and Oki*, 2002] (adapted from *Cosby et al.* [1984]), as illustrated in Figure 1. The global average value of the b parameter (not shown) decreased from 7.3 to 4.6 in the revised version, essentially resulting in less water retention and a more sandy behavior. The

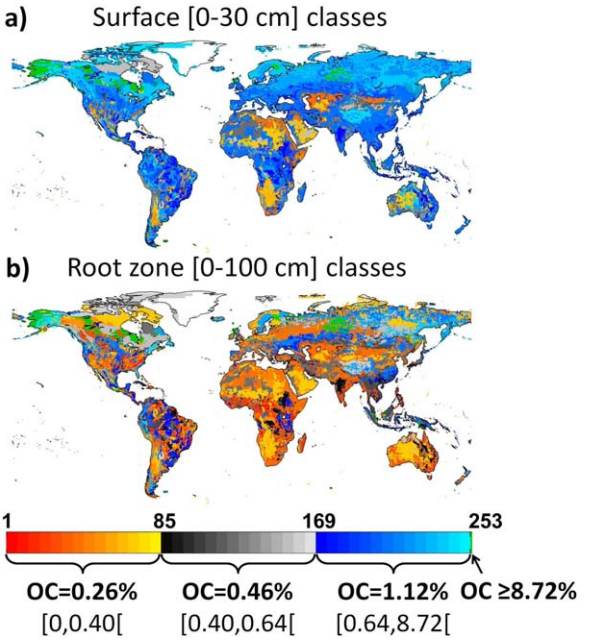

Figure 4. Global distribution of the 253 soil-organic classes at 36 km resolution for (a) the surface (0–30 cm) and (b) the root zone (0–100 cm). The first 252 classes are separated into three groups based on organic carbon content. Darker colors indicate higher clay contents. The final class ("peat") is shown in green.

global average of the revised saturated hydraulic conductivity K_s (not shown) is slightly increased. In addition, the depth-to-bedrock (not shown) is increased in most of the northern latitude areas, central and north-east Russia.

3. Impact on Simulated Hydrology

3.1. Simulations Performed

To quantify the impacts of our revised treatment of soil on the simulation of hydrological quantities, we compare three suites of offline (land only) Catchment LSM simulations. Each simulation suite covers the period January 2001 through December 2012 and was run at two different resolutions: (1) a global, 36 km simulation and (2) a 9 km simulation only for grid cells that contain in situ soil moisture measurement sites. The simulations are on the Equal Area Scalable Earth (EASE) grids, with meteorological forcings identical to those of the MERRA-Land data product, including gauge-based precipitation corrections [*Reichle*, 2012]. All simulations use a surface soil moisture layer depth of 5 cm and are preceded by spinup simulations (separately for each experiment) starting on 1 January 1991.

Table 3 summarizes the parameter versions used in the simulations. The table also connects the choice of these various versions with existing or forthcoming systems for operational products. The first two sets of simulations use "baseline" versions of the model parameters (i.e., BL and BLM2) and the third uses the "revised" version (REV). The first baseline version, "BL," does not include any of the changes presented in this paper and is effectively identical to that used for the MERRA-Land product [*Reichle et al.*, 2011], except for the depth of the surface soil moisture layer depth of 5 cm used here. The second baseline version, "BLM2," is identical to BL except (as in MERRA2) for the inclusion of the spatially interpolated depth-to-bedrock, the resetting of ν to 1.0, and the minor change in the soil moisture transport calculation. Both BL and BLM2 use the original soil texture treatment, and either one can be referred to as "baseline" when discussing the soil texture. The fully revised version "REV" is similar to BLM2 but uses the new soil texture and the corresponding new SHPs. This version is close to what will be used for the first version of the SMAP L4_SM product.

A note is warranted here regarding an error present in certain parameter versions used for the existing operational products. During the development of REV, a fitting procedure used for one of the underlying topography-related functions in the Catchment LSM was discovered to fail on occasion, affecting significantly the accurate simulation of soil moisture in about 2% or less of all land surface elements. The error typically manifests itself in excessive surface soil moisture variability and a lack of variability in root zone and total profile soil moisture. This error, which is present in the systems that produce the operational MERRA-Land and MERRA2 datasets, was removed prior to generating the 9 km simulations for BL, BLM2, and REV, the key simulations used for dataset evaluation.

3.2. Simulation of Soil Moisture

3.2.1. Soil Moisture Validation Approach

Several types of in situ measurements as well as soil moisture retrievals from the Soil Moisture Ocean Salinity (SMOS) [*Kerr et al.*, 2012] mission are used to evaluate the accuracy of simulated surface and root zone soil moisture. Our evaluation procedures consider only nonfrozen and snow-free periods (and periods for which precipitation < 1.25 mm/3 h, in case retrievals are used) and consider the following five metrics. Bias is

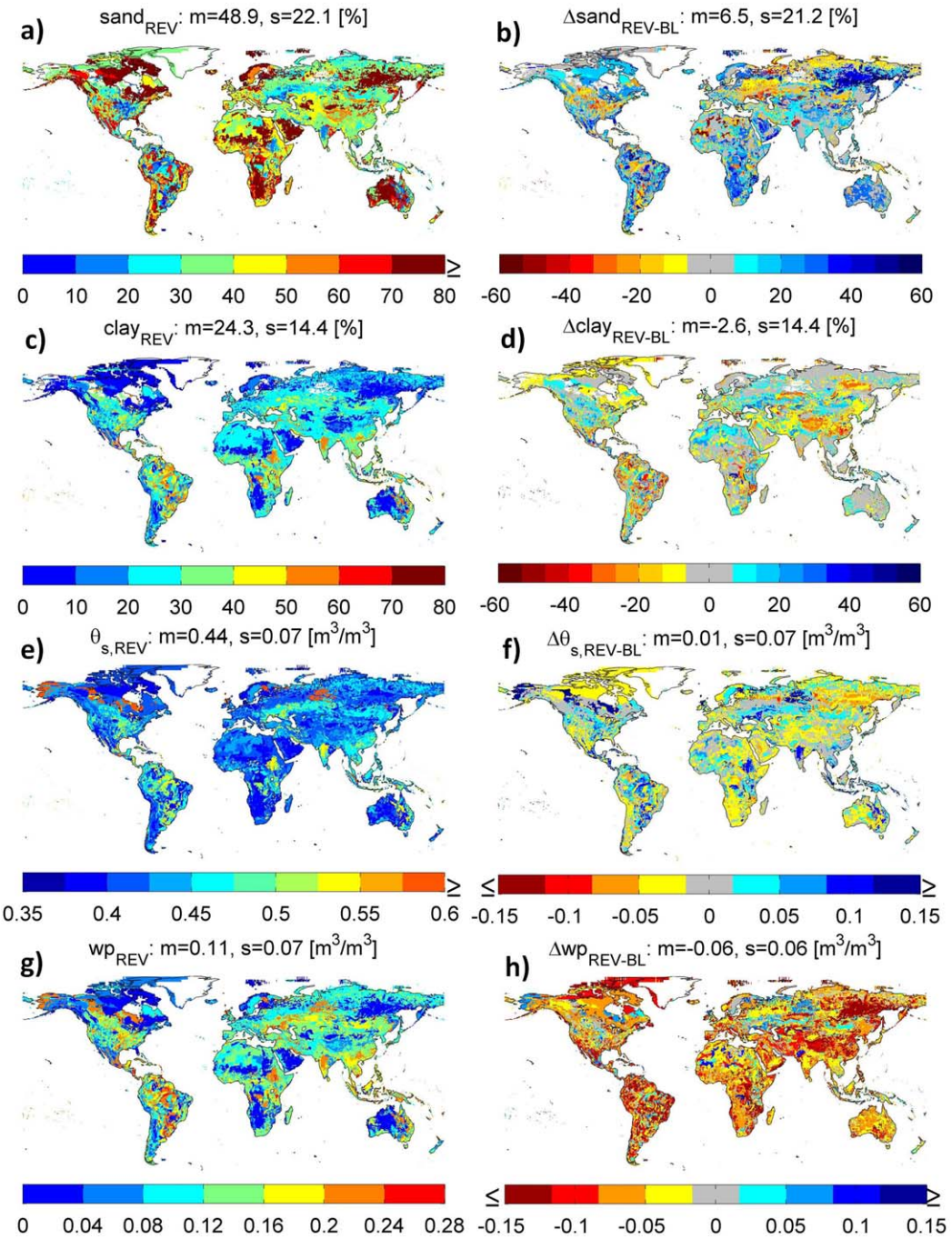

Figure 5. (a, c, e, and g) revised global root zone soil texture and parameter maps and (b, d, f, and h) difference between the revised (REV) and BL baseline version. (Figures 5a and 5b) Sand (peat class excluded), (Figures 5c and 5d) clay (peat class excluded), (Figures 5e and 5f) saturated water content θ_s, and (Figures 5g and 5h) wilting point wp. The maps are generated for 36 km grid cells. The titles indicate the global spatial mean (m) and standard deviation (s).

defined as the long-term difference between mean simulated and observed soil moisture (i.e., model minus observations). RMSE is the root-mean-square error between time series of observed and simulated soil moisture. ubRMSE is the unbiased root-mean-square error, calculated by removing the (static) long-term bias [*Entekhabi et al*., 2010b]. R is the time series correlation coefficient between observed and simulated soil moisture values. Finally, anomR is the time correlation between observed and simulated soil moisture values, calculated after removing a multiyear, 30 day smoothed, seasonally varying mean, so that correlation skill levels do not artificially reflect the seasonality of the forcing. Unless otherwise noted, all statistical metrics using

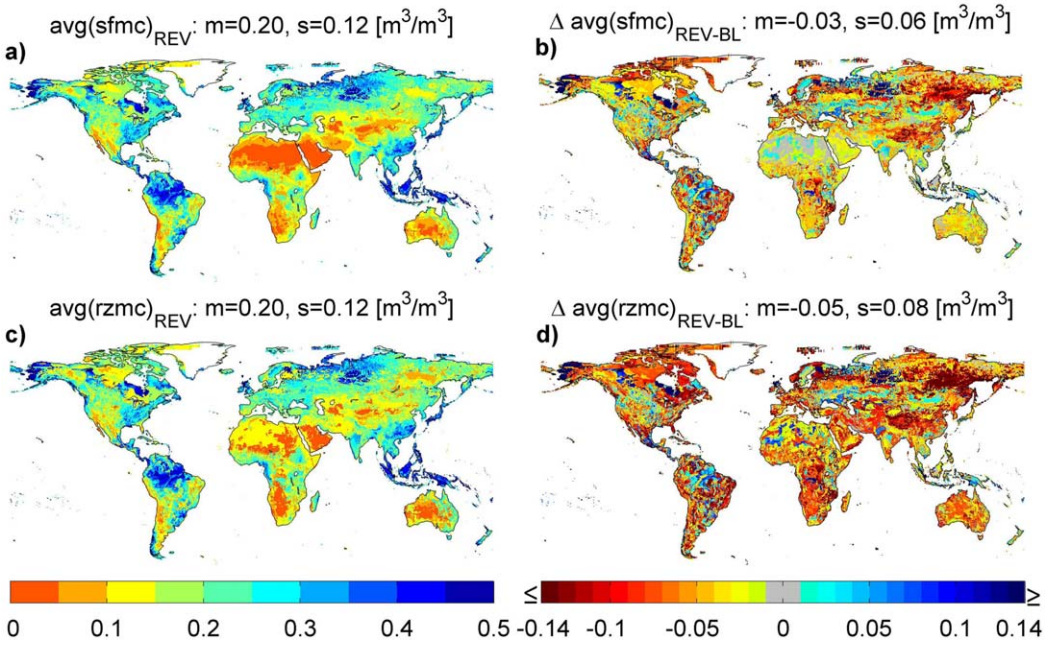

Figure 6. (a) Long-term-averaged (1 January 2001 to 1 January 2013) surface soil moisture (sfmc) obtained from a global offline simulation with the revised (REV) parameter version. (b) Differences between average surface soil moisture obtained with the revised (REV) version and that obtained with the baseline (BL) version. (c) Same as Figure 6a, but for root zone soil moisture (rzmc). (d) Same as Figure 6b, but for root zone soil moisture. The maps are generated at 36 km resolution. The titles indicate the global spatial mean (m) and standard deviation (s).

in situ measurements require a minimum of 200 data pairs in total (across all years, details below) per location. All confidence intervals (CI) are calculated for a 99% confidence level, taking into account the temporal autocorrelation in the number of degrees of freedom. Where applicable, the CIs are calculated for each validation location individually before averaging across sites. The averaged CI is computed as a simple average across all sites (that is, we do *not* assume that sites contribute independent information).

3.2.2. Global Distributions of Simulated Soil Moisture

Before comparing simulated soil moisture values with observations, a global-scale picture of the soil moistures generated with the new version is in order. Figure 6a shows the annually averaged soil moisture at the surface (0–5 cm) produced in the global 36 km simulation during the period 2001–2012 with the revised version REV. Figure 6b shows in turn how these values differ from those produced in the baseline BL simulation, and Figures 6c and 6d show the corresponding two plots for root zone (0–100 cm) moisture.

The difference plots indicate that surface moisture and (especially) root zone moisture simulated with the REV version tends to be drier than that simulated with the baseline version, with average volumetric reductions of 0.03 and 0.05 m^3/m^3 for the surface and root zones, respectively. The reductions mainly stem from a general decrease in the wilting point (Figures 1, 5g, and 5h) and a decrease in the values for the b parameter (not shown), both due to an increase in sand content and a new choice of PTFs. Increased soil moisture, on the other hand, is clearly seen in areas with high OC ("peat" class), where the assigned saturated water contents θ_s are significantly higher.

Not shown here are the impacts of the revised version on the simulated interannual variance of soil moisture. As might be expected, interannual variability of root zone soil moisture tends to be lower than that of surface soil moisture, for both the baseline and revised version. The aforementioned general reductions in mean soil moisture with the new version do not translate into correspondingly reduced standard deviations for the coarse-scale global simulation.

3.2.3. SMOS Soil Moisture Retrievals

Retrievals from passive microwave missions, like SMOS, provide an independent estimate of the global soil moisture regime. Here we use both the ascending (6:00 A.M. local time) and descending (6:00 P.M. local

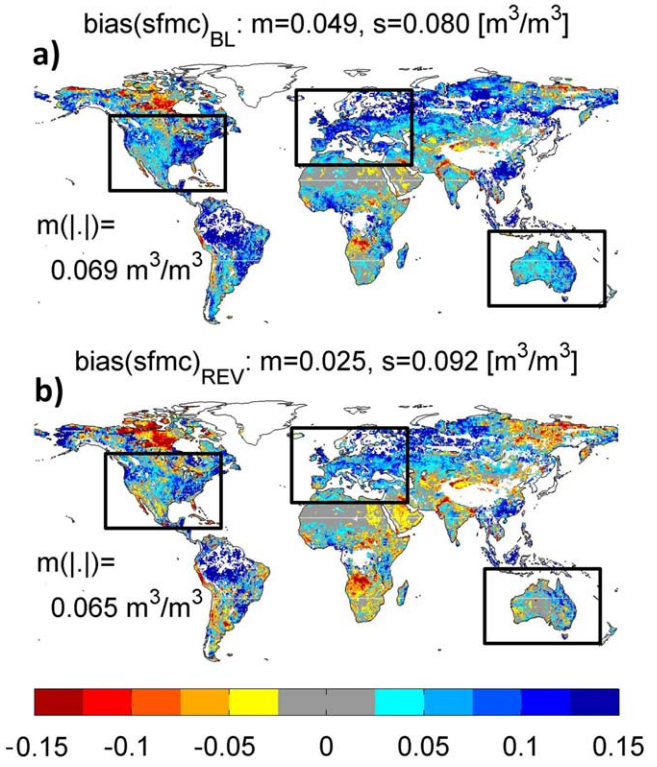

Figure 7. Long-term (1 July 2010 to 1 July 2013) bias between simulated and SMOS retrieved surface soil moisture (sfmc) for (a) the baseline (BL) version and (b) the revised (REV) version. The titles indicate the global spatial mean (m) and standard deviation (s). The global averaged absolute bias is indicated by m(|.|). The boxed areas show a decrease in bias in the REV version. The maps are generated on the 36 km grid. White areas correspond to areas with insufficient SMOS retrieval data availability.

time) SMOS retrievals as distributed in the latest available SMUDP2 product, i.e., reprocessed and produced with processor version 551. It is important to note that these retrievals are model outputs and based on a given configuration of radiative transfer modeling and auxiliary input, such as soil texture and vegetation parameters. Ideally, both satellite-based retrievals and land surface model estimates should produce similar estimates of soil moisture.

Figure 7 compares the bias between global 36 km model simulations and SMOS retrievals. Figure 7a shows that the baseline (BL) version is generally wet compared to the SMOS retrievals, with a mean bias of 0.049 m^3/m^3 and a mean absolute bias of 0.069 m^3/m^3 across the globe. After revising the LSM parameters, the situation changes: Figure 7b shows areas that are too wet and too dry compared to SMOS, with a mean bias of 0.025 m^3/m^3 and a mean absolute bias of 0.065 m^3/m^3. However, in Australia, Europe, and North America, where the soil texture information is presumably most reliable, the bias is clearly reduced. In these areas, good information about texture helps the model and retrieval soil moisture climatologies converge. The changes in ubRMSE and R are not universally positive or negative across (specific parts of) the globe (not shown). These findings are in line with the analyses below.

3.2.4. Soil Moisture Cal/Val Sites

The first in situ soil moisture measurement data set we consider, originally obtained for the purpose of calibrating and validating remote sensing observations, consists of watershed-averaged surface moisture measurements collected in four USDA-Agricultural Research Service watersheds across the U.S. [*Cosh et al.*, 2006, 2008; *Jackson et al.*, 2010]. From East to West, we refer to the four sites as LR (Little River, Georgia), LW (Little Washita, Oklahoma), WG (Walnut Gulch, Arizona), and RC (Reynolds Creek, Idaho). The exact data record varies by watershed (e.g., frozen soil moisture is measured, though not considered, at RC), but each record covers at least 10 years. The unique advantage of these data is that they represent watershed-scale averages and are thus particularly appropriate for evaluating both satellite-based retrievals and LSM soil moisture estimates.

Portions of the measured and 9 km simulated in situ time series at each of the four sites are illustrated in Figure 8. The impact of the SHP revisions is strongest in the LR, LW, and WG basins. The BL and BLM2 baseline simulations for these basins are very similar and are too wet. With the revised parameters, the bias is largely overcome, and the simulated dynamic range agrees better with that of the observations. The baseline soil moisture simulations for WG show unrealistic plateaus during dry down (indicated by arrows on the figure), which are artifacts caused by adverse interactions between the wilting point and the long-term average soil moisture in the model formulation. This deficiency is reduced with the lower wilting point value in REV. It should be noted that the in situ observations at WG (and only at WG) are postprocessed to correct

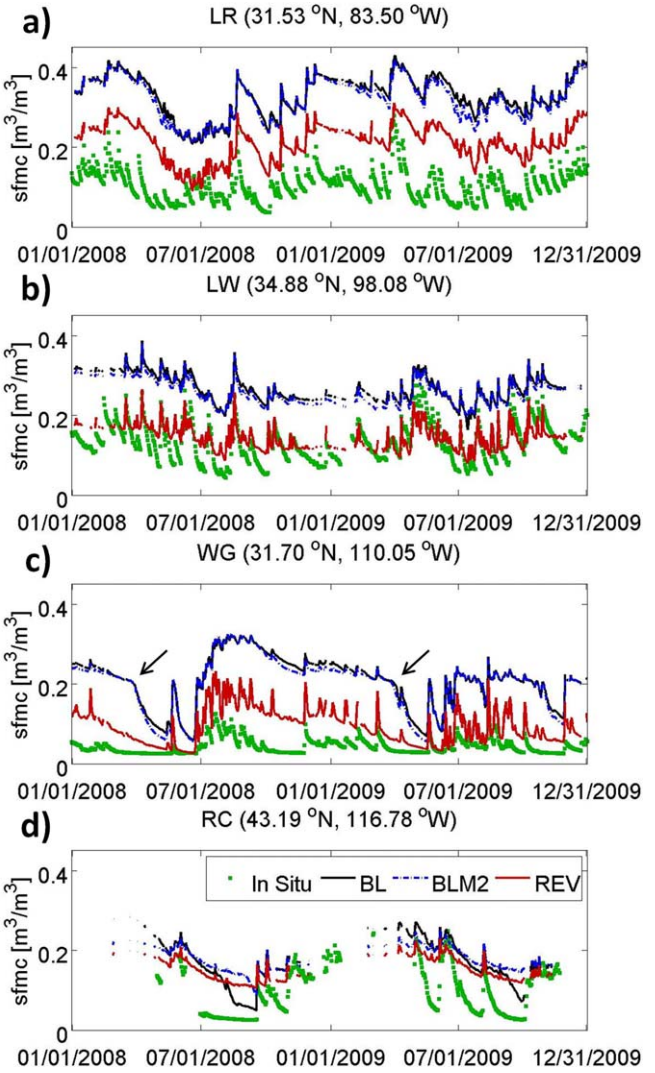

Figure 8. Surface soil moisture (sfmc) at (a) Little River. (b) Little Washita. (c) Walnut Gulch. (d) Reynolds Creek from in situ observations (green dots), the 9 km simulations with baseline parameters (BL, black lines; BLM2, blue lines) and the 9 km simulation with the revised version (REV, red lines).

for in situ observed rock fractions [*Cosh et al.*, 2008], while no such postprocessing is performed on the model simulations. The HWSD1.21 estimates the gravel percentage at about 17% in WG, and the simulated soil moisture could thus be reduced by a factor of 0.83, bringing it even closer to the observed soil moisture measurements. Finally, looking at RC, we see several gaps in the winter associated with the presence of frozen soil or snow. When measurements are available, both the baseline versions and the revised version fail to simulate the steep dry-down periods. At this site, there is a clear difference between the BL and BLM2 baseline versions because the depth-to-bedrock increased substantially and v was changed from 2.17 to 1.0 in BLM2 (and also REV).

Figure 9 summarizes the skill metrics for the four CalVal watersheds over the maximum available data record (>10 years). Again, the BL and BLM2 simulations are similar and the bias for all watersheds is substantially reduced for the revised version, with values below 0.10 m^3/m^3 for all watersheds. For the revised version, the ubRMSE is reduced to about 0.04 m^3/m^3 or less. The linear time series correlation coefficient (R and anomR, i.e., without and with mean seasonal cycles removed) has values greater than 0.7 (R) and 0.6 (anomR) for all sites with the revised version. For WG, the value for R increases significantly from 0.58 for BL to 0.76 for REV, mainly due to improved dry-down behavior. Similarly, the value for anomR increases from 0.51 for BL to 0.70 for REV.

3.2.5. Other In Situ Sites

Again, the measurements made at the above Cal/Val sites are designed to represent watershed-scale averages and are thus well suited to the evaluation of the soil moisture produced by a large-scale LSM. The more traditional in situ soil moisture measurements from sparse networks provide much more localized measurements that are generally difficult to compare directly to a model product [*Koster et al.*, 2009]. Even so, given the relatively extensive availability of the more traditional measurements, and given that many of these sites provide information on root zone soil moisture, a comparison is of value.

The measurement sites we consider here are part of the U.S. Natural Resources Conservation Service (NRCS) [*Schaefer et al.*, 2007] Soil Climate Analysis Network (SCAN), the SNOwpack TELemetry network (SNOTEL), the U.S. Climate Reference Network (USCRN) [*Diamond et al.*, 2013; *Bell et al.*, 2013], and the Oznet network in Australia's Murrumbidgee catchment [*Smith et al.*, 2012]. The data span the period 2001–2012, though the different sites have different record lengths: data from the SCAN and SNOTEL networks begin as early as 2001, whereas the USCRN data start no earlier than 2009 and the Murrumbidgee data start in either 2001

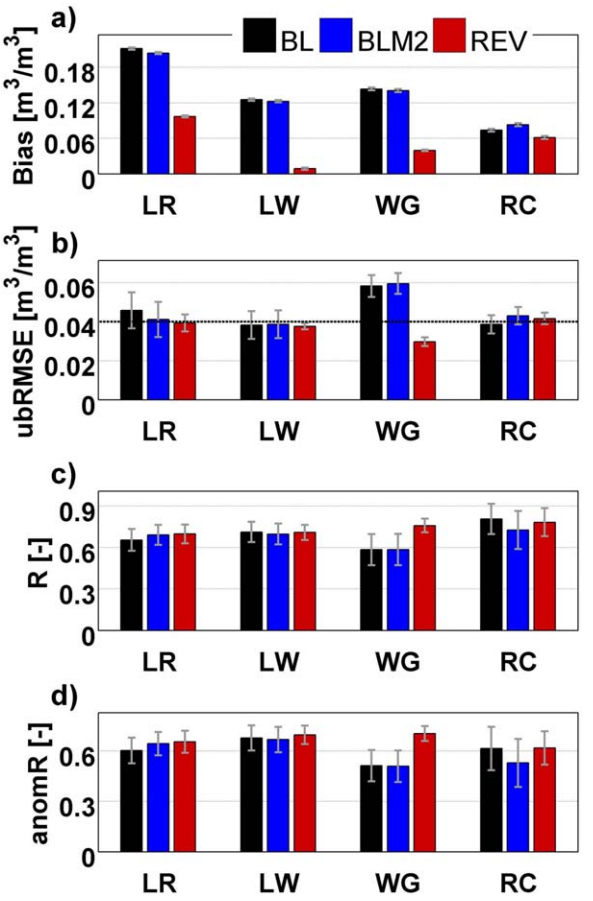

Figure 9. Surface soil moisture (a) bias (model-minus-observation), (b) unbiased root-mean-squared error (ubRMSE), (c) time series correlation coefficient (R), and (d) anomaly time series correlation coefficient (anomR) for the 9 km baseline simulations (BL, black bars; BLM2, blue bars) and the 9 km simulation with revised parameters (red bars). Metrics are for the four sites of Figure 8 and for the period January 2001 to January 2013. Also shown are 99% confidence intervals.

or 2009, depending on location. An extensive quality control is applied to the data to remove irregularities. Only periods with a consistent climatology are retained—we exclude periods with distinct sensor calibrations or with settling or malfunctioning sensors. The surface soil moisture evaluation uses observational data at 5 cm depth. The root zone soil moisture evaluation uses a mean value of the data at 5, 10, 20, and 50 cm depth, except for the Oznet sites where only the measurements at 20 cm depth are used, because the data within individual layers are insufficiently available to produce a consistent profile estimate.

Table 4 summarizes the soil moisture skill metrics for the four networks and for both surface and root zone soil moisture. Except for the bias (and consequently also the RMSE), none of the metrics shows a statistically significant change due to parameter changes in any of the networks. This indicates that the soil parameters have a greater impact on the mean value of soil moisture and thus on the bias. The temporal variability is apparently driven more by the time variability of the meteorological forcings.

Figure 10 shows the bias (model-minus-observation), averaged across all sites within each network. The sites in the sparse networks give a statistically significant (at the 99% confidence level) indication that the surface (Figure 10a) and the root zone (Figure 10b) soil moistures are too wet for both baseline simulations. Bias values for BL range between 0.06 and 0.07 m^3/m^3 for surface soil moisture and between 0.03 and 0.05 m^3/m^3 for root zone soil moisture. The BLM2 simulations are only slightly improved compared to the BL simulations. More striking, though, is the significant bias reduction obtained through the use of the revised soil texture and SHPs (REV), with bias values ranging between 0.03 and 0.05 m^3/m^3 for the surface and between -0.01 and -0.002 m^3/m^3 for the root zone. Note again that the CIs are calculated for individual sites and then averaged. The number of daily data pairs at the in situ sites varies between the imposed minimum amount of 200 and a maximum of 4153 (most sites have less than 1000 data pairs). The CIs are therefore larger than those shown in Figure 9 (also, note different range in vertical axis) for the individual Cal/Val sites which all have more than 2000 daily data pairs.

3.3. Simulation of Hydrological Fluxes

Figures 11a and 11b show, respectively, the global distributions of differences in total runoff (surface runoff plus base flow) and latent heat flux between the simulations using the revised and baseline BL parameter versions, averaged over the period 2001–2012, and at a 36 km resolution. The main impact of the revisions is a reduction in latent heat flux in midlatitudes and an increase in latent heat flux in many tropical areas, with corresponding opposite changes in runoff production. These changes, however, are arguably small. The global average of evaporation over land is 43 W/m^2 for the revised simulation, reduced by 1% from that of the baseline simulations. This reduction is much smaller than the uncertainty of observations-based estimates in the literature [*Schlosser and Gao*, 2010]. At individual locations, the magnitudes of change in

Table 4. Surface and Root Zone Soil Moisture Skills and 99% Confidence Intervals (CI) for Baseline and Revised Simulations Averaged Over Individual Sites in Four Sparse Networks: SCAN, SNOTEL, USCRN, and Oznet[a]

	Surface Soil Moisture					Root Zone Soil Moisture				
		BL	BLM2	REV			BL	BLM2	REV	
	N	Bias (m^3/m^3)			CI	N	Bias (m^3/m^3)			CI
SCAN	141	0.068	0.064	**0.040**	0.004	110	0.029	0.018	**−0.013**	±0.004
SNOTEL	221	0.055	0.054	**0.026**	0.007	12	0.043	0.037	**−0.004**	±0.005
USCRN	87	0.064	0.061	0.053	0.006	65	0.036	0.023	**−0.002**	±0.005
Oznet	29	0.072	0.071	**0.038**	0.004	29	0.050	0.047	**−0.003**	±0.003
	N	RMSE (m^3/m^3)			CI	N	RMSE (m^3/m^3)			CI
SCAN	141	0.118	0.115	**0.099**	0.004	110	0.094	0.089	0.081	±0.004
SNOTEL	221	0.119	0.117	0.109	0.005	12	0.099	0.096	0.094	±0.004
USCRN	87	0.112	0.110	0.118	0.004	65	0.110	0.105	0.097	±0.004
Oznet	29	0.098	0.097	**0.076**	0.003	29	0.091	0.088	**0.078**	±0.003
	N	ubRMSE (m^3/m^3)			CI	N	ubRMSE (m^3/m^3)			CI
SCAN	141	0.056	0.056	0.058	0.007	110	0.041	0.039	0.041	±0.008
SNOTEL	221	0.066	0.066	0.068	0.008	12	0.046	0.047	0.046	±0.008
USCRN	87	0.056	0.056	0.055	0.009	65	0.040	0.040	0.041	±0.011
Oznet	29	0.053	0.054	0.055	0.005	29	0.053	0.054	0.054	±0.004
	N	R			CI	N	R			CI
SCAN	141	0.638	0.639	0.607	0.151	109	0.687	0.681	0.663	±0.241
SNOTEL	221	0.656	0.655	0.638	0.181	12	0.604	0.581	0.646	±0.264
USCRN	87	0.711	0.706	0.682	0.187	65	0.744	0.740	0.725	±0.337
Oznet	29	0.730	0.710	0.695	0.115	29	0.743	0.742	0.738	±0.186
	N	anomR			CI	N	anomR			CI
SCAN	139	0.562	0.563	0.531	0.137	105	0.604	0.597	0.566	±0.227
SNOTEL	217	0.553	0.552	0.536	0.181	12	0.507	0.485	0.490	±0.339
USCRN	75	0.660	0.659	0.633	0.149	50	0.687	0.680	0.675	±0.256
Oznet	29	0.631	0.609	0.595	0.107	29	0.667	0.672	0.664	±0.153

[a]All metrics use daily averaged soil moisture during the period 1 January 2001 to 1 January 2013. Root zone soil moisture is defined as a weighted profile-average of four layers down to 50 cm depth, except for the Oznet sites where a single layer at 20 cm depth is used. N refers to the number of sites used per network. Bold numbers highlight the simulations with the best performance.

midlatitude latent heat flux tend to lie below 5 W/m^2; local estimates of annual evaporation obtained with different observations-based approaches often differ by much larger values [e.g., *Ferguson et al*., 2010]. Surface temperature changes (not shown) are also small, generally below a few tenths of a degree, and with positive surface temperature changes generally appearing, as expected, in regions of reduced latent heat flux. The temporal variability of latent heat (not shown) is generally reduced with the revised parameters. Large-scale evaporation rates cannot be directly measured, but the REV simulation's field of latent heat flux is on average slightly closer (not shown) to the model-based upscaled estimates of *Jung et al*. [2011], which are based on FLUXNET [*Baldocchi et al*., 2001] latent heat observations.

For some large-scale hydrological basins, naturalized streamflow measurements allow an assessment of simulated runoff. The simulation using the baseline BL parameter version produces basin-level runoff ratios (ratio of total runoff to precipitation, not shown) that are too small compared to such observational estimates. The ratios simulated in the BL simulation are, in fact, quite close to those produced by *Koster and Mahanama* [2012], who used a very similar version of the model. In line with the above findings, the changes induced by the revised soil parameters (the new SHPs and, for example, the revised v parameter) bring the simulated runoff ratios closer to the observations—that is, the new parameters adjust the runoff ratios in the right direction, reducing the RMSE of runoff ratio by about 20%. This improvement is obviously only partial. As implied by *Koster and Mahanama* [2012], a proper reproduction of observed runoff ratios would require changes in the formulation of the model physics rather than a simple modification of soil parameters. We do not implement such formulation changes here, and thus we do not expect the simulated runoff bias to be eliminated.

In parallel with the analyses of *Mahanama et al*. [2012] and *Reichle et al*. [2012], we also quantified the accuracy of simulated streamflows using anomaly correlations against the time series of measured (and naturalized) streamflows in the aforementioned basins. Much more often than not, anomR values for the REV simulation were higher than those for the BL simulation (not shown). However, the large uncertainties

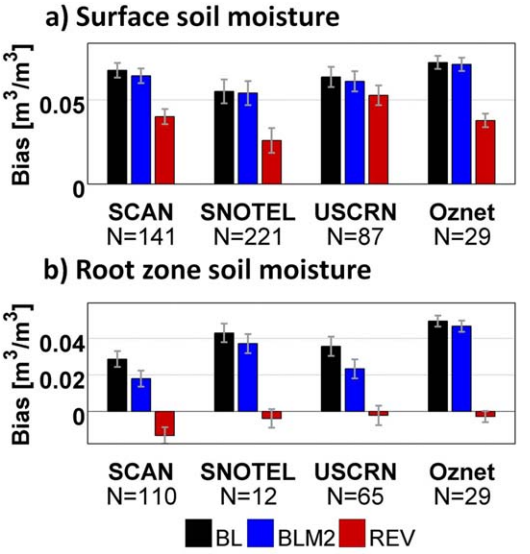

Figure 10. Bias values and 99% confidence intervals for (a) surface and (b) root zone soil moisture estimates from 9 km simulations using baseline (BL, black bars; BLM2, blue bars) and revised (REV, red bars) parameters. Bias values are averaged over individual sites in four sparse networks: SCAN, SNOTEL, USCRN, and Oznet. Bias is defined as simulated minus observed soil moisture, after taking the long-term average of daily soil moisture over the period 1 January 2001 to 1 January 2013. Root zone soil moisture is defined as a weighted profile-average of four layers down to 50 cm depth, except for the Oznet sites where a single layer at 20 cm depth is used. N refers to the number of sites used per network.

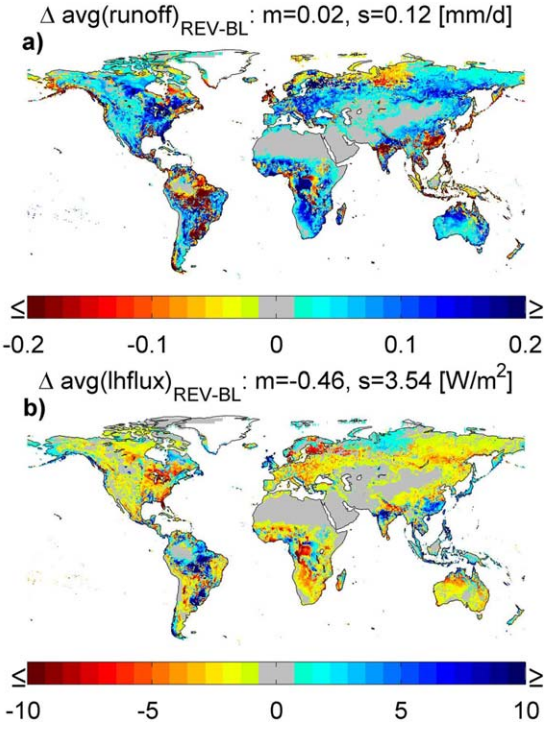

Figure 11. Differences in long-term-averaged (1 January 2001 to 1 January 2013) (a) runoff and (b) latent heat flux (lhflux) between 36 km simulations using revised (REV) and baseline (BL) parameters. The titles indicate the global spatial mean (m) and standard deviation (s).

associated with the limited evaluation period preclude any statistically significant conclusions about streamflow improvement in the context of an anomR metric.

4. Conclusions

We introduce in this paper a revised treatment of soil texture and associated soil hydraulic parameters (SHPs) for use in large-scale land surface models. The revised treatment makes use of newer and more detailed soil texture data sets (including organic matter information) and translates the texture data into SHPs using the best available pedotransfer functions from the literature. The result is a much more comprehensive and presumably more accurate characterization of soil properties across the globe.

The impacts of the changes on simulated hydrology are quantified using global and continental-scale simulations with the Catchment LSM of the NASA GEOS-5 modeling system. The revised version of the model parameters generally leads to improved soil moisture simulation, with (for example) a greatly reduced bias and ubRMSE when processed against high-quality surface soil moisture observations in four CalVal watersheds in the U.S., and with a significantly reduced bias when compared to sparse observational networks. The revised parameters also yield a soil moisture climatology that is closer to that of SMOS retrievals in areas where the soil texture information is presumably more accurate. Furthermore, simulations using the revised parameters produce more runoff and less evaporation, moving these fluxes slightly closer to values suggested by independent streamflow and FLUXNET estimates.

The revised soil treatment is expected to be a part of future versions of the GEOS-5 system. As part of GEOS-5, the new soil texture and SHPs will help provide improved background information for the creation of SMAP products, including the L4_SM product. However, the usefulness of the new soil treatment is not limited to GEOS-5-based applications. Large-scale land surface models used for global or continental-scale simulation typically require the type of soil texture and/or soil hydraulic property information developed

here. Model developers in general may find it useful to consider our soil treatment as a potential option for their own systems.

Appendix A

A lists with SHPs for all soil classes is provided in Table A1. The parameter values are derived for "topsoil", using the Wösten et al. (2001a) PFTs for the first 252 classes and lookup values for the peat class (class 253). The soil class numbers for OC category 1 (1-84) are shown in Figure 1b; the numbers for OC category 2 (85-168) and 3 (169-252) follow the same ordering in the soil triangle. Table A1 also includes the wilting point (wp) and field capacity (fc), obtained by inverting the Campbell (1974) formulation at −1500 and −33 kPa underpressure (equivalent to pF=4.3 and 2.5), respectively.

Table A1. Revised SHP for All Soil Classes[a]

Class	Cl (wt %)	Sa (wt %)	OC (wt %)	θ_s^* (m^3/m^3)	ρ_b (g/cm^3)	θ_s (m^3/m^3)	b	ψ_s (m)	K_s (m/s)	wp (m^3/m^3)	fc (m^3/m^3)
1	53.33	43.33	0.26	0.47	1.32	0.47	4.94	−0.28	2.10E-05	0.130	0.28
2	56.67	36.67	0.26	0.49	1.26	0.50	5.41	−0.40	1.42E-05	0.165	0.33
3	53.33	33.33	0.26	0.48	1.27	0.50	6.21	−0.37	9.85E-06	0.189	0.35
4	56.67	26.67	0.26	0.50	1.21	0.52	6.01	−0.54	8.84E-06	0.205	0.39
5	53.33	23.33	0.26	0.50	1.22	0.52	6.33	−0.50	7.34E-06	0.211	0.39
6	56.67	16.67	0.26	0.52	1.16	0.55	5.91	−0.74	6.84E-06	0.222	0.42
7	53.33	13.33	0.26	0.52	1.17	0.54	6.08	−0.67	5.81E-06	0.222	0.42
8	56.67	6.67	0.26	0.54	1.10	0.57	5.54	−1.00	5.45E-06	0.228	0.45
9	53.33	3.33	0.26	0.54	1.12	0.56	5.66	−0.90	4.56E-06	0.225	0.44
10	43.33	53.33	0.26	0.43	1.43	0.42	5.02	−0.15	2.09E-05	0.107	0.23
11	46.67	46.67	0.26	0.44	1.38	0.45	5.81	−0.19	1.41E-05	0.143	0.28
12	43.33	43.33	0.26	0.44	1.38	0.45	6.42	−0.20	9.60E-06	0.161	0.29
13	46.67	36.67	0.26	0.46	1.33	0.48	6.60	−0.26	8.61E-06	0.181	0.32
14	43.33	33.33	0.26	0.46	1.34	0.47	6.68	−0.27	7.01E-06	0.183	0.32
15	46.67	26.67	0.26	0.48	1.29	0.49	6.66	−0.35	6.56E-06	0.198	0.35
16	43.33	23.33	0.26	0.47	1.30	0.49	6.57	−0.36	5.45E-06	0.195	0.35
17	46.67	16.67	0.26	0.49	1.24	0.51	6.43	−0.46	5.15E-06	0.208	0.38
18	43.33	13.33	0.26	0.49	1.25	0.50	6.30	−0.47	4.21E-06	0.201	0.37
19	46.67	6.67	0.26	0.51	1.19	0.53	6.07	−0.61	3.97E-06	0.212	0.40
20	43.33	3.33	0.26	0.50	1.21	0.52	5.93	−0.60	3.15E-06	0.204	0.39
21	33.33	63.33	0.26	0.40	1.50	0.39	4.45	−0.11	2.13E-05	0.077	0.18
22	36.67	56.67	0.26	0.41	1.47	0.41	5.41	−0.13	1.40E-05	0.112	0.23
23	33.33	53.33	0.26	0.41	1.47	0.42	5.77	−0.14	9.41E-06	0.125	0.24
24	36.67	46.67	0.26	0.43	1.43	0.43	6.23	−0.17	8.31E-06	0.146	0.27
25	33.33	43.33	0.26	0.42	1.44	0.43	6.09	−0.19	6.64E-06	0.145	0.27
26	36.67	36.67	0.26	0.44	1.40	0.45	6.39	−0.23	6.16E-06	0.163	0.30
27	33.33	33.33	0.26	0.44	1.40	0.45	6.08	−0.26	5.02E-06	0.157	0.29
28	36.67	26.67	0.26	0.45	1.36	0.46	6.29	−0.31	4.72E-06	0.173	0.32
29	33.33	23.33	0.26	0.45	1.37	0.46	5.92	−0.34	3.77E-06	0.164	0.31
30	36.67	16.67	0.26	0.46	1.32	0.48	6.06	−0.40	3.56E-06	0.179	0.34
31	33.33	13.33	0.26	0.46	1.34	0.47	5.68	−0.44	2.75E-06	0.168	0.33
32	36.67	6.67	0.26	0.48	1.28	0.49	5.76	−0.51	2.59E-06	0.182	0.35
33	33.33	3.33	0.26	0.47	1.30	0.48	5.39	−0.56	1.93E-06	0.170	0.34
34	23.33	73.33	0.26	0.39	1.54	0.37	3.45	−0.10	2.28E-05	0.045	0.14
35	26.67	66.67	0.26	0.39	1.52	0.39	4.41	−0.11	1.45E-05	0.075	0.18
36	23.33	63.33	0.26	0.39	1.52	0.40	4.55	−0.13	9.59E-06	0.084	0.19
37	26.67	56.67	0.26	0.40	1.50	0.41	5.15	−0.15	8.21E-06	0.106	0.22
38	23.33	53.33	0.26	0.40	1.50	0.41	4.87	−0.18	6.45E-06	0.102	0.22
39	26.67	46.67	0.26	0.41	1.48	0.42	5.36	−0.20	5.84E-06	0.121	0.25
40	23.33	43.33	0.26	0.41	1.48	0.42	4.94	−0.24	4.66E-06	0.112	0.24
41	26.67	36.67	0.26	0.42	1.45	0.43	5.34	−0.27	4.30E-06	0.130	0.27
42	23.33	33.33	0.26	0.42	1.46	0.42	4.87	−0.32	3.37E-06	0.119	0.26
43	26.67	26.67	0.26	0.43	1.42	0.44	5.22	−0.35	3.13E-06	0.136	0.28
44	23.33	23.33	0.26	0.42	1.44	0.43	4.72	−0.43	2.37E-06	0.124	0.28
45	26.67	16.67	0.26	0.44	1.40	0.44	5.03	−0.46	2.21E-06	0.140	0.30
46	23.33	13.33	0.26	0.43	1.41	0.44	4.54	−0.56	1.61E-06	0.127	0.29
47	26.67	6.67	0.26	0.45	1.37	0.45	4.80	−0.59	1.49E-06	0.142	0.31
48	23.33	3.33	0.26	0.44	1.39	0.44	4.33	−0.71	1.04E-06	0.128	0.31
49	13.33	83.33	0.26	0.40	1.52	0.37	2.38	−0.11	2.67E-05	0.018	0.09
50	16.67	76.67	0.26	0.39	1.53	0.38	3.17	−0.12	1.61E-05	0.039	0.13

Table A1. (continued)

Class	Cl (wt %)	Sa (wt %)	OC (wt %)	θ_s^* (m^3/m^3)	ρ_b (g/cm^3)	θ_s (m^3/m^3)	b	ψ_s (m)	K_s (m/s)	wp (m^3/m^3)	fc (m^3/m^3)
51	13.33	73.33	0.26	0.39	1.52	0.39	3.19	−0.15	1.05E-05	0.044	0.15
52	16.67	66.67	0.26	0.39	1.52	0.39	3.77	−0.15	8.57E-06	0.063	0.17
53	13.33	63.33	0.26	0.39	1.52	0.39	3.46	−0.20	6.63E-06	0.058	0.17
54	16.67	56.67	0.26	0.40	1.52	0.40	3.97	−0.21	5.76E-06	0.076	0.20
55	13.33	53.33	0.26	0.39	1.52	0.40	3.55	−0.27	4.51E-06	0.067	0.20
56	16.67	46.67	0.26	0.40	1.51	0.40	4.01	−0.28	4.02E-06	0.084	0.22
57	13.33	43.33	0.26	0.40	1.51	0.40	3.54	−0.37	3.08E-06	0.073	0.21
58	16.67	36.67	0.26	0.40	1.50	0.41	3.97	−0.39	2.79E-06	0.090	0.24
59	13.33	33.33	0.26	0.40	1.51	0.40	3.48	−0.51	2.06E-06	0.078	0.23
60	16.67	26.67	0.26	0.41	1.48	0.41	3.86	−0.52	1.88E-06	0.094	0.25
61	13.33	23.33	0.26	0.40	1.50	0.40	3.38	−0.69	1.33E-06	0.081	0.25
62	16.67	16.67	0.26	0.41	1.47	0.41	3.73	−0.69	1.22E-06	0.097	0.27
63	13.33	13.33	0.26	0.41	1.49	0.41	3.25	−0.92	8.30E-07	0.084	0.27
64	16.67	6.67	0.26	0.42	1.45	0.42	3.57	−0.91	7.60E-07	0.099	0.29
65	13.33	3.33	0.26	0.41	1.47	0.41	3.11	−1.22	4.94E-07	0.086	0.29
66	3.33	93.33	0.26	0.43	1.43	0.40	1.52	−0.16	3.44E-05	0.004	0.05
67	6.67	86.67	0.26	0.41	1.47	0.39	2.06	−0.15	1.96E-05	0.014	0.09
68	3.33	83.33	0.26	0.42	1.46	0.41	2.04	−0.19	1.25E-05	0.015	0.10
69	6.67	76.67	0.26	0.40	1.49	0.40	2.48	−0.19	9.70E-06	0.027	0.12
70	3.33	73.33	0.26	0.41	1.48	0.40	2.22	−0.25	7.36E-06	0.023	0.13
71	6.67	66.67	0.26	0.40	1.51	0.40	2.64	−0.25	6.08E-06	0.035	0.15
72	3.33	63.33	0.26	0.40	1.51	0.40	2.30	−0.34	4.66E-06	0.028	0.15
73	6.67	56.67	0.26	0.39	1.52	0.39	2.69	−0.35	3.97E-06	0.041	0.17
74	3.33	53.33	0.26	0.39	1.52	0.40	2.31	−0.48	2.98E-06	0.033	0.17
75	6.67	46.67	0.26	0.39	1.53	0.39	2.69	−0.49	2.59E-06	0.046	0.19
76	3.33	43.33	0.26	0.39	1.54	0.39	2.29	−0.68	1.87E-06	0.037	0.19
77	6.67	36.67	0.26	0.39	1.53	0.39	2.65	−0.69	1.65E-06	0.051	0.21
78	3.33	33.33	0.26	0.38	1.55	0.39	2.24	−0.98	1.14E-06	0.041	0.22
79	6.67	26.67	0.26	0.39	1.54	0.39	2.58	−0.96	1.01E-06	0.054	0.24
80	3.33	23.33	0.26	0.38	1.55	0.38	2.18	−1.40	6.70E-07	0.044	0.26
81	6.67	16.67	0.26	0.39	1.53	0.39	2.49	−1.34	5.99E-07	0.058	0.27
82	3.33	13.33	0.26	0.38	1.55	0.38	2.10	−1.99	3.78E-07	0.048	0.30
83	6.67	6.67	0.26	0.39	1.53	0.39	2.39	−1.85	3.40E-07	0.061	0.30
84	3.33	3.33	0.26	0.38	1.55	0.38	2.01	−2.80	2.05E-07	0.052	0.35
85	53.33	43.33	0.46	0.46	1.31	0.47	5.16	−0.27	2.12E-05	0.136	0.29
86	56.67	36.67	0.46	0.48	1.26	0.50	5.67	−0.38	1.43E-05	0.172	0.34
87	53.33	33.33	0.46	0.48	1.26	0.50	6.49	−0.35	1.00E-05	0.196	0.35
88	56.67	26.67	0.46	0.50	1.20	0.52	6.30	−0.51	8.96E-06	0.212	0.39
89	53.33	23.33	0.46	0.50	1.21	0.52	6.60	−0.48	7.52E-06	0.218	0.39
90	56.67	16.67	0.46	0.52	1.15	0.55	6.19	−0.70	6.99E-06	0.229	0.42
91	53.33	13.33	0.46	0.52	1.16	0.54	6.34	−0.64	6.00E-06	0.228	0.42
92	56.67	6.67	0.46	0.54	1.10	0.57	5.79	−0.94	5.61E-06	0.235	0.45
93	53.33	3.33	0.46	0.54	1.11	0.56	5.88	−0.85	4.74E-06	0.232	0.44
94	43.33	53.33	0.46	0.43	1.42	0.43	5.19	−0.15	2.15E-05	0.112	0.23
95	46.67	46.67	0.46	0.45	1.37	0.45	6.03	−0.19	1.44E-05	0.149	0.28
96	43.33	43.33	0.46	0.45	1.37	0.46	6.64	−0.20	9.93E-06	0.167	0.30
97	46.67	36.67	0.46	0.46	1.32	0.48	6.84	−0.25	8.88E-06	0.187	0.33
98	43.33	33.33	0.46	0.46	1.33	0.48	6.91	−0.26	7.31E-06	0.189	0.33
99	46.67	26.67	0.46	0.48	1.27	0.50	6.90	−0.34	6.82E-06	0.205	0.36
100	43.33	23.33	0.46	0.48	1.28	0.49	6.79	−0.35	5.73E-06	0.201	0.35
101	46.67	16.67	0.46	0.50	1.23	0.51	6.66	−0.45	5.39E-06	0.214	0.38
102	43.33	13.33	0.46	0.49	1.24	0.51	6.50	−0.45	4.45E-06	0.208	0.37
103	46.67	6.67	0.46	0.51	1.18	0.53	6.28	−0.59	4.18E-06	0.219	0.40
104	43.33	3.33	0.46	0.51	1.19	0.52	6.11	−0.58	3.35E-06	0.210	0.39
105	33.33	63.33	0.46	0.40	1.49	0.40	4.57	−0.11	2.22E-05	0.081	0.19
106	36.67	56.67	0.46	0.42	1.45	0.42	5.56	−0.13	1.46E-05	0.117	0.23
107	33.33	53.33	0.46	0.42	1.45	0.42	5.93	−0.14	9.90E-06	0.130	0.25
108	36.67	46.67	0.46	0.43	1.42	0.44	6.41	−0.17	8.72E-06	0.152	0.28
109	33.33	43.33	0.46	0.43	1.42	0.44	6.26	−0.19	7.05E-06	0.151	0.28
110	36.67	36.67	0.46	0.44	1.38	0.46	6.57	−0.23	6.52E-06	0.169	0.30
111	33.33	33.33	0.46	0.44	1.38	0.45	6.25	−0.25	5.36E-06	0.163	0.30
112	36.67	26.67	0.46	0.46	1.34	0.47	6.47	−0.30	5.02E-06	0.179	0.32
113	33.33	23.33	0.46	0.45	1.35	0.47	6.09	−0.33	4.06E-06	0.170	0.32
114	36.67	16.67	0.46	0.47	1.30	0.48	6.23	−0.39	3.81E-06	0.185	0.34
115	33.33	13.33	0.46	0.47	1.31	0.48	5.84	−0.43	2.98E-06	0.174	0.33
116	36.67	6.67	0.46	0.48	1.26	0.50	5.92	−0.49	2.79E-06	0.188	0.36
117	33.33	3.33	0.46	0.48	1.27	0.49	5.54	−0.54	2.10E-06	0.176	0.35
118	23.33	73.33	0.46	0.39	1.51	0.38	3.54	−0.10	2.42E-05	0.048	0.14

Table A1. (continued)

Class	Cl (wt %)	Sa (wt %)	OC (wt %)	θ_s^* (m^3/m^3)	ρ_b (g/cm^3)	θ_s (m^3/m^3)	b	ψ_s (m)	K_s (m/s)	wp (m^3/m^3)	fc (m^3/m^3)
119	26.67	66.67	0.46	0.40	1.50	0.39	4.52	−0.11	1.53E-05	0.080	0.19
120	23.33	63.33	0.46	0.40	1.50	0.40	4.66	−0.13	1.02E-05	0.089	0.20
121	26.67	56.67	0.46	0.41	1.48	0.41	5.28	−0.15	8.74E-06	0.111	0.23
122	23.33	53.33	0.46	0.41	1.47	0.41	4.99	−0.18	6.94E-06	0.107	0.23
123	26.67	46.67	0.46	0.42	1.45	0.42	5.49	−0.20	6.26E-06	0.126	0.25
124	23.33	43.33	0.46	0.42	1.45	0.42	5.05	−0.24	5.05E-06	0.118	0.25
125	26.67	36.67	0.46	0.43	1.42	0.44	5.48	−0.26	4.65E-06	0.136	0.27
126	23.33	33.33	0.46	0.42	1.43	0.43	4.99	−0.31	3.67E-06	0.125	0.27
127	26.67	26.67	0.46	0.44	1.40	0.44	5.35	−0.34	3.41E-06	0.142	0.29
128	23.33	23.33	0.46	0.43	1.40	0.44	4.84	−0.41	2.61E-06	0.129	0.28
129	26.67	16.67	0.46	0.45	1.37	0.45	5.16	−0.44	2.42E-06	0.146	0.31
130	23.33	13.33	0.46	0.44	1.38	0.45	4.66	−0.52	1.78E-06	0.132	0.30
131	26.67	6.67	0.46	0.46	1.33	0.46	4.93	−0.55	1.65E-06	0.148	0.32
132	23.33	3.33	0.46	0.45	1.35	0.45	4.44	−0.66	1.16E-06	0.133	0.31
133	13.33	83.33	0.46	0.40	1.49	0.38	2.45	−0.12	2.85E-05	0.020	0.10
134	16.67	76.67	0.46	0.40	1.50	0.39	3.25	−0.12	1.71E-05	0.042	0.14
135	13.33	73.33	0.46	0.40	1.49	0.40	3.27	−0.15	1.13E-05	0.047	0.15
136	16.67	66.67	0.46	0.40	1.50	0.40	3.86	−0.15	9.23E-06	0.067	0.18
137	13.33	63.33	0.46	0.40	1.49	0.40	3.55	−0.19	7.19E-06	0.062	0.18
138	16.67	56.67	0.46	0.40	1.49	0.41	4.07	−0.20	6.25E-06	0.080	0.20
139	13.33	53.33	0.46	0.40	1.49	0.41	3.64	−0.26	4.94E-06	0.071	0.20
140	16.67	46.67	0.46	0.41	1.48	0.41	4.11	−0.28	4.40E-06	0.089	0.22
141	13.33	43.33	0.46	0.41	1.48	0.41	3.63	−0.35	3.40E-06	0.077	0.22
142	16.67	36.67	0.46	0.41	1.46	0.42	4.06	−0.37	3.08E-06	0.094	0.24
143	13.33	33.33	0.46	0.41	1.47	0.41	3.56	−0.48	2.30E-06	0.082	0.24
144	16.67	26.67	0.46	0.42	1.45	0.42	3.96	−0.49	2.09E-06	0.099	0.26
145	13.33	23.33	0.46	0.41	1.46	0.42	3.46	−0.63	1.50E-06	0.085	0.26
146	16.67	16.67	0.46	0.42	1.43	0.43	3.82	−0.64	1.37E-06	0.101	0.28
147	13.33	13.33	0.46	0.42	1.44	0.42	3.33	−0.83	9.38E-07	0.087	0.27
148	16.67	6.67	0.46	0.43	1.41	0.43	3.66	−0.82	8.58E-07	0.103	0.29
149	13.33	3.33	0.46	0.43	1.43	0.42	3.19	−1.08	5.62E-07	0.089	0.29
150	3.33	93.33	0.46	0.43	1.40	0.41	1.58	−0.16	3.68E-05	0.005	0.06
151	6.67	86.67	0.46	0.42	1.45	0.40	2.14	−0.15	2.10E-05	0.016	0.09
152	3.33	83.33	0.46	0.42	1.43	0.41	2.12	−0.19	1.35E-05	0.018	0.11
153	6.67	76.67	0.46	0.41	1.46	0.40	2.56	−0.19	1.05E-05	0.030	0.13
154	3.33	73.33	0.46	0.42	1.45	0.41	2.31	−0.25	8.02E-06	0.026	0.13
155	6.67	66.67	0.46	0.41	1.47	0.41	2.72	−0.25	6.64E-06	0.038	0.16
156	3.33	63.33	0.46	0.41	1.47	0.41	2.38	−0.33	5.13E-06	0.031	0.16
157	6.67	56.67	0.46	0.41	1.48	0.40	2.77	−0.34	4.38E-06	0.045	0.18
158	3.33	53.33	0.46	0.40	1.48	0.41	2.38	−0.46	3.31E-06	0.036	0.18
159	6.67	46.67	0.46	0.40	1.49	0.40	2.76	−0.46	2.88E-06	0.049	0.20
160	3.33	43.33	0.46	0.40	1.50	0.40	2.36	−0.63	2.10E-06	0.039	0.20
161	6.67	36.67	0.46	0.40	1.49	0.40	2.71	−0.63	1.85E-06	0.053	0.22
162	3.33	33.33	0.46	0.40	1.50	0.40	2.30	−0.88	1.29E-06	0.043	0.22
163	6.67	26.67	0.46	0.40	1.49	0.40	2.64	−0.87	1.15E-06	0.057	0.24
164	3.33	23.33	0.46	0.40	1.51	0.40	2.23	−1.23	7.65E-07	0.046	0.25
165	6.67	16.67	0.46	0.40	1.49	0.40	2.55	−1.18	6.85E-07	0.059	0.27
166	3.33	13.33	0.46	0.40	1.50	0.40	2.15	−1.69	4.36E-07	0.049	0.29
167	6.67	6.67	0.46	0.41	1.48	0.40	2.44	−1.58	3.91E-07	0.062	0.29
168	3.33	3.33	0.46	0.40	1.50	0.39	2.06	−2.31	2.38E-07	0.051	0.33
169	53.33	43.33	1.12	0.46	1.30	0.46	5.79	−0.25	1.81E-05	0.153	0.30
170	56.67	36.67	1.12	0.48	1.25	0.49	6.44	−0.34	1.20E-05	0.190	0.34
171	53.33	33.33	1.12	0.48	1.25	0.50	7.27	−0.32	8.79E-06	0.214	0.36
172	56.67	26.67	1.12	0.50	1.19	0.52	7.14	−0.45	7.78E-06	0.230	0.39
173	53.33	23.33	1.12	0.50	1.19	0.52	7.38	−0.43	6.78E-06	0.236	0.40
174	56.67	16.67	1.12	0.52	1.14	0.54	6.99	−0.61	6.24E-06	0.247	0.43
175	53.33	13.33	1.12	0.52	1.13	0.54	7.05	−0.57	5.56E-06	0.247	0.42
176	56.67	6.67	1.12	0.54	1.08	0.57	6.51	−0.81	5.14E-06	0.253	0.46
177	53.33	3.33	1.12	0.55	1.07	0.56	6.50	−0.75	4.50E-06	0.249	0.45
178	43.33	53.33	1.12	0.43	1.38	0.43	5.66	−0.15	1.95E-05	0.127	0.25
179	46.67	46.67	1.12	0.45	1.34	0.45	6.63	−0.19	1.29E-05	0.165	0.29
180	43.33	43.33	1.12	0.45	1.33	0.46	7.25	−0.19	9.26E-06	0.184	0.31
181	46.67	36.67	1.12	0.47	1.29	0.48	7.52	−0.24	8.19E-06	0.205	0.34
182	43.33	33.33	1.12	0.47	1.28	0.49	7.53	−0.25	6.99E-06	0.207	0.34
183	46.67	26.67	1.12	0.49	1.24	0.50	7.57	−0.32	6.45E-06	0.223	0.37
184	43.33	23.33	1.12	0.49	1.23	0.50	7.40	−0.33	5.61E-06	0.220	0.37
185	46.67	16.67	1.12	0.51	1.18	0.52	7.29	−0.42	5.23E-06	0.233	0.39
186	43.33	13.33	1.12	0.51	1.18	0.52	7.05	−0.42	4.47E-06	0.226	0.39
187	46.67	6.67	1.12	0.53	1.13	0.54	6.83	−0.54	4.15E-06	0.237	0.41

Table A1. (continued)

Class	Cl (wt %)	Sa (wt %)	OC (wt %)	θ_s^* (m^3/m^3)	ρ_b (g/cm^3)	θ_s (m^3/m^3)	b	ψ_s (m)	K_s (m/s)	wp (m^3/m^3)	fc (m^3/m^3)
188	43.33	3.33	1.12	0.53	1.13	0.54	6.59	−0.53	3.44E-06	0.228	0.41
189	33.33	63.33	1.12	0.42	1.43	0.41	4.90	−0.12	2.13E-05	0.094	0.20
190	36.67	56.67	1.12	0.43	1.41	0.43	5.99	−0.13	1.39E-05	0.132	0.25
191	33.33	53.33	1.12	0.43	1.39	0.44	6.37	−0.15	9.76E-06	0.146	0.27
192	36.67	46.67	1.12	0.44	1.36	0.45	6.92	−0.17	8.52E-06	0.169	0.29
193	33.33	43.33	1.12	0.45	1.35	0.46	6.73	−0.19	7.12E-06	0.169	0.30
194	36.67	36.67	1.12	0.46	1.32	0.47	7.10	−0.22	6.52E-06	0.187	0.32
195	33.33	33.33	1.12	0.46	1.31	0.47	6.73	−0.25	5.54E-06	0.181	0.32
196	36.67	26.67	1.12	0.47	1.27	0.49	6.99	−0.29	5.15E-06	0.198	0.34
197	33.33	23.33	1.12	0.48	1.27	0.49	6.55	−0.31	4.29E-06	0.189	0.34
198	36.67	16.67	1.12	0.49	1.23	0.50	6.72	−0.36	3.99E-06	0.204	0.36
199	33.33	13.33	1.12	0.49	1.23	0.50	6.27	−0.39	3.22E-06	0.193	0.35
200	36.67	6.67	1.12	0.51	1.18	0.52	6.35	−0.45	2.99E-06	0.206	0.38
201	33.33	3.33	1.12	0.51	1.18	0.51	5.93	−0.48	2.32E-06	0.194	0.37
202	23.33	73.33	1.12	0.41	1.45	0.40	3.78	−0.11	2.42E-05	0.058	0.16
203	26.67	66.67	1.12	0.42	1.44	0.41	4.82	−0.12	1.53E-05	0.092	0.20
204	23.33	63.33	1.12	0.42	1.42	0.42	4.99	−0.14	1.05E-05	0.103	0.22
205	26.67	56.67	1.12	0.43	1.40	0.43	5.65	−0.15	8.97E-06	0.126	0.25
206	23.33	53.33	1.12	0.43	1.39	0.44	5.35	−0.18	7.34E-06	0.123	0.25
207	26.67	46.67	1.12	0.44	1.37	0.45	5.89	−0.19	6.59E-06	0.143	0.27
208	23.33	43.33	1.12	0.44	1.36	0.45	5.42	−0.23	5.48E-06	0.135	0.27
209	26.67	36.67	1.12	0.45	1.34	0.46	5.88	−0.25	5.01E-06	0.154	0.29
210	23.33	33.33	1.12	0.45	1.33	0.46	5.36	−0.29	4.08E-06	0.142	0.29
211	26.67	26.67	1.12	0.46	1.30	0.47	5.75	−0.31	3.76E-06	0.160	0.31
212	23.33	23.33	1.12	0.46	1.30	0.47	5.21	−0.37	2.96E-06	0.147	0.31
213	26.67	16.67	1.12	0.48	1.27	0.48	5.55	−0.39	2.73E-06	0.164	0.33
214	23.33	13.33	1.12	0.48	1.27	0.48	5.01	−0.45	2.06E-06	0.149	0.32
215	26.67	6.67	1.12	0.49	1.23	0.49	5.29	−0.48	1.89E-06	0.165	0.34
216	23.33	3.33	1.12	0.49	1.23	0.49	4.78	−0.55	1.37E-06	0.150	0.33
217	13.33	83.33	1.12	0.42	1.41	0.40	2.67	−0.12	2.94E-05	0.028	0.12
218	16.67	76.67	1.12	0.42	1.43	0.41	3.51	−0.12	1.77E-05	0.053	0.16
219	13.33	73.33	1.12	0.43	1.41	0.42	3.56	−0.15	1.20E-05	0.060	0.18
220	16.67	66.67	1.12	0.43	1.41	0.42	4.16	−0.15	9.81E-06	0.081	0.20
221	13.33	63.33	1.12	0.43	1.39	0.43	3.85	−0.19	7.86E-06	0.076	0.20
222	16.67	56.67	1.12	0.43	1.39	0.43	4.39	−0.20	6.83E-06	0.095	0.23
223	13.33	53.33	1.12	0.44	1.38	0.44	3.94	−0.25	5.54E-06	0.086	0.23
224	16.67	46.67	1.12	0.44	1.37	0.44	4.43	−0.26	4.94E-06	0.105	0.25
225	13.33	43.33	1.12	0.44	1.37	0.44	3.93	−0.32	3.92E-06	0.092	0.24
226	16.67	36.67	1.12	0.45	1.35	0.45	4.38	−0.33	3.54E-06	0.111	0.26
227	13.33	33.33	1.12	0.45	1.35	0.45	3.86	−0.41	2.71E-06	0.096	0.26
228	16.67	26.67	1.12	0.45	1.33	0.45	4.28	−0.42	2.46E-06	0.114	0.28
229	13.33	23.33	1.12	0.45	1.33	0.45	3.75	−0.52	1.81E-06	0.099	0.27
230	16.67	16.67	1.12	0.46	1.30	0.46	4.13	−0.52	1.65E-06	0.117	0.29
231	13.33	13.33	1.12	0.46	1.31	0.46	3.62	−0.64	1.16E-06	0.101	0.29
232	16.67	6.67	1.12	0.47	1.28	0.47	3.97	−0.63	1.05E-06	0.117	0.31
233	13.33	3.33	1.12	0.47	1.28	0.46	3.47	−0.78	7.11E-07	0.101	0.30
234	3.33	93.33	1.12	0.46	1.32	0.43	1.78	−0.18	3.82E-05	0.010	0.08
235	6.67	86.67	1.12	0.44	1.36	0.42	2.38	−0.16	2.20E-05	0.024	0.12
236	3.33	83.33	1.12	0.45	1.33	0.44	2.38	−0.21	1.45E-05	0.027	0.14
237	6.67	76.67	1.12	0.44	1.37	0.43	2.84	−0.19	1.14E-05	0.041	0.16
238	3.33	73.33	1.12	0.45	1.35	0.44	2.58	−0.25	8.87E-06	0.037	0.16
239	6.67	66.67	1.12	0.44	1.37	0.44	3.00	−0.25	7.40E-06	0.051	0.18
240	3.33	63.33	1.12	0.45	1.35	0.44	2.65	−0.32	5.85E-06	0.043	0.18
241	6.67	56.67	1.12	0.44	1.37	0.44	3.05	−0.32	5.03E-06	0.058	0.20
242	3.33	53.33	1.12	0.44	1.36	0.44	2.65	−0.41	3.89E-06	0.047	0.20
243	6.67	46.67	1.12	0.44	1.37	0.44	3.04	−0.41	3.40E-06	0.062	0.22
244	3.33	43.33	1.12	0.44	1.36	0.44	2.61	−0.53	2.54E-06	0.050	0.22
245	6.67	36.67	1.12	0.44	1.36	0.44	2.98	−0.52	2.25E-06	0.065	0.24
246	3.33	33.33	1.12	0.44	1.36	0.44	2.54	−0.68	1.61E-06	0.053	0.24
247	6.67	26.67	1.12	0.45	1.35	0.44	2.90	−0.67	1.43E-06	0.068	0.25
248	3.33	23.33	1.12	0.45	1.35	0.44	2.46	−0.88	9.81E-07	0.054	0.26
249	6.67	16.67	1.12	0.45	1.34	0.44	2.80	−0.84	8.76E-07	0.069	0.27
250	3.33	13.33	1.12	0.45	1.34	0.44	2.38	−1.11	5.74E-07	0.056	0.28
251	6.67	6.67	1.12	0.46	1.32	0.45	2.69	−1.04	5.13E-07	0.070	0.29
252	3.33	3.33	1.12	0.45	1.33	0.44	2.28	−1.38	3.21E-07	0.056	0.30
253	n/a	n/a	≥8.72	n/a	n/a	0.80	3.41	−1.76	7.86E-07	0.216	0.66

[a]The parameters are derived using the *Wösten et al.* [1999, 2001a] PTFs, with topsoil=1, for the first 252 classes. The "peat" class is assigned lookup table values from the Staring series for "peat_B16." The symbols are explained in section 2.3.

Acknowledgment
The authors thank Mike Cosh for providing the USDA/ARS CalVal soil moisture validation data set, Narendra Das and Steven Chan for discussions on compositing texture databases, Lien Loosvelt, Henk Wösten, Keith Saxton, and Wim Cornelis for helpful discussions on the calculation of soil hydraulic parameters, and the anonymous reviewers for their helpful comments. The research was supported by the NASA Soil Moisture Active Passive mission, the NASA Modeling, Analysis, and Prediction program, and the NASA High-End Computing program. The soil texture data and soil hydraulic parameters used and developed for the baseline and revised simulations in this paper are available at the Global Modeling and Assimilation Office in NASA Goddard Space Flight Center, Maryland, USA. The STATSGO2 soil texture data are available from the USDA/NRCS (http://websoilsurvey.nrcs.usda.gov/), and the HWSD1.21 soil texture data are available from the International Institute for Applied Systems Analysis (IIASA) (http://webarchive.iiasa.ac.at/Research/LUC/External-World-soil-database/HTML/).

References

Albergel, C., G. Balsamo, P. de Rosnay, J. Munoz-Sabater, and S. Boussetta (2012), A bare ground evaporation revision in the ECMWF land-surface scheme: Evaluation of its impact using ground soil moisture and satellite microwave data, *Hydrol. Earth Syst. Sci.*, *16*, 3607–3620.

Baldocchi, D., et al. (2001), FLUXNET: A new tool to study the temporal and spatial variability of ecosystem-scale carbon dioxide, water vapor, and energy flux densities, Bull. *Am. Meteorol. Soc.*, *82*(11), 2415–2434.

Balsamo, G., P. Viterbo, A. Belkaars, B. van den Hurk, M. Hirschi, A. K. Betts, and K. Scipal (2009), A revised hydrology for the ECMWF model: Verification from field site to terrestrial water storage and impact in theintegrated forecast system, *J. Hydrometeorol.*, *10*, 623–643, doi: 10.1175/2008JHM1068.1.

Baroni, G., A. Facchi, C. Gandolfi, B. Ortuani, D. Horeschi, and J. C. van Dam (2010), Uncertainty in the determination of soil hydraulic parameters and its influence on the performance of two hydrological models of different complexity, *Hydrol. Earth Syst. Sci.*, *14*(2), 251–270.

Batjes, N. H. (2012), ISRIC-WISE derived soil properties on a 5 by 5 arc-minutes global grid (ver. 1.2), *ISRIC Rep. 2012/01*, 52 p., ISRIC—World Soil Inf., Wageningen, Netherlands. [Available at www.isric.org.]

Bell, J., et al. (2013), U.S. climate reference network soil moisture and temperature observations, *J. Hydrometeorol.*, *14*, 977–988.

Bormann, H. (2010), Towards a hydrologically motivated soil texture classification, *Geoderma*, *157*, 142–153.

Campbell, G. (1974), A simple method for determining unsaturated conductivity from moisture retention data, *Soil Sci.*, *117*, 311–314.

Comer, R., and M. Best (2012), Revisiting GLACE: Understanding the role of the land surface in land atmosphere coupling, *J. Hydrometeorol.*, *13*, 1704–1718.

Cosby, B., G. Hornberger, R. Clapp, and T. Ginn (1984), A statisticsl exploration of the relationships of soil moisture characteristics to the physical propertie of soil, *Water Resour. Res.*, *20*(6), 682–690.

Cosh, M. H., T. J. Jackson, P. Starks, and G. Heathman (2006), Temporal stability of surface soil moisture in the Little Washita River watershed and its applications in satellite soil moisture validation, *J. Hydrol.*, *323*(1-4), 168–177.

Cosh, M. H., T. J. Jackson, S. Moran, and R. Bindlish (2008), Temporal persistence and stability of surface soil moisture in a semi-arid watershed, *Remote Sens. Environ.*, *112*, 304–313.

Cronican, A. E., and M. M. Gribb (2004), Literature review: Equations for predicting hydraulic conductivity based on grain-size data. Supplement to Technical Note entitled: Hydraulic conductivity prediction for sandy soils, in *Ground Water*, *42*(3), 459–464.

Dai, Y., W. Shangguan, Q. Duan, B. Liu, S. Fu, and G. Niu (2013), Development of a China dataset of soil hydraulic parameters using pedotransfer functions for land surface modeling, *J. Hydrometeorol.*, *14*, 869–887.

De Lannoy, G. J. M., R. H. Reichle, and V. R. N. Pauwels (2013), Global calibration of the GEOS-5 L-band microwave radiative transfer model over nonfrozen land using SMOS observations, *J. Hydrometeorol.*, *14*(3), 765–785, doi:10.1175/JHM-D-12-092.1.

Dharssi, I., P. L. Vidale, A. Verhoef, B. Macpherson, C. Jones, and M. Best (2009), New soil physical properties implemented in the Unified Model at PS18, *Met R&D Tech. Rep. 528*, 34 p, Met Office, Exeter, U. K.

Diamond, H., et al. (2013), U.S. climate reference network after one decade of operations: Status and assessment, *Bull. Am. Meteorol. Soc.*, *94*, 485–498.

Dirmeyer, P. (2000), Using a global soil wetness dataset to improve seasonal climate simulation, *J. Clim.*, *13*(16), 2900–2922.

Dirmeyer, P., and T. Oki (2002), *The Second Global Soil Wetness Project (GSWP-2) Science and Implementation Plan, IGPO Publ. Ser.*, vol. *37*, 64 p, IGPO, Columbia, Md.

Ducharne, A., R. D. Koster, M. J. Suarez, M. Stieglitz, and P. Kumar (2000), A catchment-based approach to modeling land surface processes in a general circulation model: 2. Parameter estimation and model demonstration, *J. Geophys. Res.*, *105*(D20), 24,838–24,838.

Entekhabi, D., et al. (2010a), The Soil Moisture Active and Passive (SMAP) mission, *Proc. IEEE*, *98*(5), 704–716.

Entekhabi, D., R. H. Reichle, R. D. Koster, and W. T. Crow (2010b), Performance metrics for soil moisture retrievals and application requirements, *J. Hydrometeorol.*, *11*, 832–840, doi:10.1175/2010JHM1223.1.

FAO/IIASA/ISRIC/ISSCAS/JRC (2012), Harmonized World Soil Database (version 1.2), Food and Agric. Organ., Rome. (Available at: http://webarchive.iiasa.ac.at/Research/LUC/External-World-soil-database/HTML/)

FAO/UNESCO (1971–1981), The FAO-UNESCO soil map of the World, U. N. Educ., Sci. Cultural Organ., Paris, France.

Farouki, O. (1981), Thermal properties of soils, *CRRL Monogr.*, 81-1, Hanover, New Hampshire, USA, 134p.

Ferguson, C. R., J. Sheffield, E. F. Wood, and H. Gao (2010), Quantifying uncertainty in a remote sensing-based estimate of evapotranspiration over continental USA, *Int. J. Remote Sens.*, *31*, 3821–3865.

Harrison, K. W., S. V. Kumar, C. D. Peters-Lidard, and J. A. Santanello (2012), Quantifying the change in soil moisture modeling uncertainty from remote sensing observations using Bayesian inference techniques, *Water Resour. Res.*, *48*, W11514, doi:10.1029/2012WR012337.

Jackson, T. J., M. H. Cosh, R. Bindlish, P. J. Starks, D. D. Bosch, M. Seyfried, D. C. Goodrich, M. S. Moran, and J. Du (2010), Validation of advances microwave scanning radiometer soil moisture, *IEEE Trans. Geosci. Remote Sens.*, *48*(2), 4256–4272.

Jung, M., et al. (2011), Global patterns of land-atmosphere fluxes of carbon dioxide, latent heat, and sensible heat derived from eddy covariance, satellite, and meteorological observations, *J. Geophys. Res.*, *116*, D00J07, doi:10.1029/2010JG001566.

Kay, B. D., A. P. da Silva, and J. A. Baldock (1997), Sensitivity of soil structure to changes in organic carbon content: Predictions using pedotransfer functions, *Can. J. Soil Sci.*, *77*, 655–667.

Kerr, Y. H., et al. (2012), The SMOS soil moisture retrieval algorithm, *IEEE Trans. Geosci. Remote Sens.*, *50*(5), 1384–1403.

Koster, R. D., and S. P. P. Mahanama (2012), Land surface controls on hydroclimatic means and variability, *J. Hydrometeorol.*, *13*, 1604–1620.

Koster, R. D., M. J. Suarez, A. Ducharne, M. Stieglitz, and P. Kumar (2000), A catchment-based approach to modeling land surface processes in a general circulation model: 1. Model structure, *J. Geophys. Res.*, *105*(D20), 24,809–24,822.

Koster, R. D., et al. (2004), Regions of strong coupling between soil moisture and precipitation, *Science*, *305*(5687), 1138–1140.

Koster, R. D., Z. Guo, R. Yang, P. A. Dirmeyer, K. Mitchell, and M. J. Puma (2009), On the nature of soil moisture in land surface models, *J. Clim.*, *22*, 4322–4335.

Lawrence, D. M., and A. G. Slater (2000), Incorporating organic soil into a global climate model, *Clim. Dyn.*, *30*, 145–160.

Letts, M. G., N. T. Roulet, N. T.Comer, M. Skarupa, and D. L. Verseghy (2000), Parametrization of peatland hydraulic properties for the canadian land surface scheme, *Atmos. Ocean*, *38*(1), 141–160.

Liu, S., Y. Wei, W. M. Post, R. B. Cook, K. Schaefer, and M. M. Thornton (2013), The unified North American soil map and its implication on the soil organic carbon stock in North America, *Biogeosciences*, *10*, 2915–2930.

Loosvelt, L., V. R. N. Pauwels, W. M. Cornelis, G. J. M. De Lannoy, and N. E. C. Verhoest (2011), Impact of soil hydraulic parameter uncertainty on soil moisture modeling, *Water Resour. Res.*, *47*, W03505, doi:10.1029/2010WR009204.

Mahanama, S., B. Livneh, R. Koster, D. Lettenmaier, and R. Reichle (2012), Soil moisture, snow, and seasonal streamflow forecasts in the United States, *J. Hydrometeorol.*, *13*, 189–203.

McCuen, R. H., W. J. Rawls, and D. L. Brakensiek (1981), Statistical analysis of the Brooks-Corey and the Green-Ampt parameters across soil textures, *Water Resour. Res.*, *17*(4), 1005–1013.
McKenzie, N., K. Coughland, and H. Cresswell (2002), *Soil Physical Measurement and Interpretation for Land Evaluation, Aust. Soil Land Surv. Handb. Ser.*, vol. *5*, CSIRO Publ., Melbourne, Australia.
Minasny, B., and A. E. Hartemink (2011), Predicting soil properties in the tropics, *Earth Sci. Rev.*, *106*, 52–62.
NRCS Soil Survey Staff, USDA (2012), General Soil Map (STATSGO2) (United States), Washington, D. C. [Available at http://websoilsurvey.nrcs.usda.gov/, last accessed May 2013.], USA.
Pauwels, V., A. Balenzano, G. Satalino, H. Skriver, N. E. C. Verhoest, and F. Mattia (2009), Optimization of soil hydraulic model parameters using synthetic aperture radar data: An integrated multidisciplinary approach, *IEEE Trans. Geosci. Remote Sens.*, *47*(2), 455–467.
Rawls, W., and D. Brakensiek (1989), Estimation of soil water retention and hydraulic properties, in *Unsaturated Flow in Hydrologic Modeling—Theory and Practice*, edited by H. Morel-Seytoux, pp. 275–200, Kluwer Acad., Norwell, Mass.
Rawls, W., D. Brakensiek, and K. E. Saxton (1982), Estimation of soil water properties, *Trans. ASAE*, *25*(5), 1316–1320.
Rawls, W., Y. Pachepsky, J. Ritchie, T. Sobeckic, and H. Bloodworth (2003), Effect of soil organic carbon on soil water retention, *Geoderma*, *116*, 61–76.
Reichle, R., W. Crow, R. Koster, J. Kimball, and G. De Lannoy (2012), SMAP algorithm theoretical basis document: L4 surface and root zone soil moisture product, *Tech. Rep. JPL D-66483*, Jet Propul. Lab., Pasadena, Calif.
Reichle, R. H. (2012), The MERRA-land data product (version 1.2), *GMAO Off. Note 3*, NASA Global Model. and Assimilation Off. [Available at http://gmao.gsfc.nasa.gov/pubs/office_notes/.], Greenbelt, Md.
Reichle, R. H., R. D. Koster, G. J. M. De Lannoy, B. Forman, Q. Liu, S. P. P. Mahanama, and A. Toure (2011), Assessment and enhancement of MERRA land surface hydrology estimates, *J. Clim.*, *24*, 6322–6338.
Reichle, R. H., G. J. M. De Lannoy, B. A. Forman, C. S. Draper, and Q. Liu (2014), Connecting satellite observations with water cycle variables through land data assimilation: Examples using the NASA GEOS-5 LDAS, *Surv. Geophys.*, *35*, 577–606, doi:10.1007/s10712-013-9220-8.
Reynolds, C., T. J. Jackson, and W. J. Rawls (2000), Estimating soil water-holding capacities by linking the Food and Agriculture Organization soil map of the world with global pedon databases and continuous pedotransfer functions, *Water Resour. Res.*, *36*(12), 3653–3662.
Richards, L. A. (1931), Capillary conduction of liquids through porous mediums, *Physics*, *1*(5), 318–333, doi:10.1063/1.1745010.
Rienecker, M. M., et al. (2011), MERRA: NASA's modern-era retrospective analysis for research and applications, *J. Clim.*, *24*(14), 3624–3648, doi:10.1175/JCLI-D-11-00015.1.
Salvucci, G. D., and D. Entekhabi (2011), An alternate and robust approach to calibration for the estimation of land surface model parameters based on remotely sensed observations, *Geophys. Res. Lett.*, *38*, L16404, doi:10.1029/2011GL048366.
Santanello, J., C. D. Peters-Lidard, M. E. Garcia, D. M. Mocko, M. A. Tischler, M. S. Moran, and D. P. Thoma (2007), Using remotely-sensed estimates of soil moisture to infer soil texture and hydraulic properties across a semi-arid watershed, *Remote Sens. Environ.*, *110*(1), 79–97.
Saxton, K., and W. Rawls (2006), Soil water characteristic estimates by texture and organic matter for hydrologic solutions, *Soil Sci. Soc. Am. J.*, *70*, 1569–1578.
Schaefer, G. L., M. H. Cosh, and T. J. Jackson (2007), The USDA natural resources conservation service soil climate analysis network (SCAN), *J. Atmos. Oceanic Technol.*, *24*(12), 2073–2077.
Schlosser, C. A., and X. Gao (2010), Assessing evapotranspiration estimates from the second Global Soil Wetness Project (GSWP-2) simulations, *J. Hydrometeorol.*, *11*, 880–896.
Shangguan, W., Y. Dai, Q. Duan, B. Liu, and H. Yuan (2014), A global soil dataset for earth system modeling, *J. Adv. Model. Earth Syst.*, *6*, 249–263, doi:10.1002/2013MS000293.
Sivapalan, M., K. Beven, and E. F. Wood (1987), On hydrologic similarity: 2. A scaled model of storm runoff production, *Water Resour. Res.*, *23*(12), 2266–2278.
Smith, A. B., J. P. Walker, A. W. Western, R. I. Young, K. M. Ellett, R. Pipunic, R. Grayson, L. Siriwidena, F. Chiew, and H. Richter (2012), The Murrumbidgee soil moisture monitoring network data set, *Water Resour. Res.*, *48*, W07701, doi:10.1029/2012WR011976.
USDA Soil Survey Staff, Bureau of Plant Industry, Soils and Agricultural Engineering (1951), *Soil Survey Manual, USDA Handbook*, vol *18*, Washington, D. C.
van Genuchten, M. (1980), A closed-form equation for predicting the hydraulic conductivity of unsaturated soils, *Soil Sci. Soc. Am. J.*, *44*, 892–898.
Wagner, B., V. Tarnawski, V. Hennings, U. Müller, G.Wessolek, and R. Plagge (2001), Evaluation of pedo-transfer functions for unsaturated soil hydraulic conductivity using an independent data set, *Geoderma*, *102*, 275–297.
Wesseling, J. G., C. R. Stoof, C. J. Ritsema, K. Oostindie, and L. W. Dekker (2009), The effect of soil texture and organic amendment on the hydrological behaviour of coarse-textured soils, *Soil Use Manage.*, *25*, 274–283.
Wood, A. W., and D. Lettenmaier (2006), A test ved for new seasonal hydrologic forecasting approaches in the western United States, *Bull. Am. Meteorol. Soc.*, *87*, 1699–1712.
Wösten, J., A. Lilly, A. Nemes, and C. LeBas (1999), Development and use of a database of hydraulic properties of European soils, *Geoderma*, *90*, 169–185.
Wösten, J., Y. A. Pachepsky, and W. Rawls (2001a), Pedotransfer functions: Bridging the gap between available basic soil data and missing soil hydraulic characteristics, *J. Hydrol.*, *251*, 123–150.
Wösten, J., G. Veerman, W. de Groot, and J. Stolte (2001b), Waterretentie- en doorlatendheidskarakteristieken van boven- en ondergronden in Nederland; de Staringreeks. vernieuwde uitgave 2001, *Alterra Rapp. 153*, Alterra, Res. Inst. voor de Groene Ruimte, Wageningen, Netherlands.